Mathematics and Mechanics of Solids
XX(X):1–26

Reprints and permission:
sagepub.co.uk/journalsPermissions.nav
DOI: 10.1177/ToBeAssigned
www.sagepub.com/
SAGE

# Effective properties of hierarchical fiber-reinforced composites via a three-scale asymptotic homogenization approach

**Ariel Ramírez-Torres[1], Raimondo Penta[2], Reinaldo Rodríguez-Ramos[3] and Alfio Grillo[1]**

**Abstract**

The study of the properties of multiscale composites is of great interest in engineering and biology. Particularly, hierarchical composite structures can be found in nature and in engineering. During the past decades, the multiscale asymptotic homogenization technique has shown its potential in the description of such composites by taking advantage of their characteristics at the smaller scales, ciphered in the so-called *effective coefficients*. Here, we extend previous works by studying the in-plane and out-of-plane effective properties of hierarchical linear elastic solid composites via a three-scale asymptotic homogenization technique. In particular, the approach is adjusted for a multiscale composite with a square-symmetric arrangement of uniaxially aligned cylindrical fibers, and the formulae for computing its effective properties are provided. Finally, we show the potential of the proposed asymptotic homogenization procedure by modeling the effective properties of musculoskeletal mineralized tissues, and compare the results with theoretical and experimental data for bone and tendon tissues.

**Keywords**

Hierarchical composites, Three-scale asymptotic homogenization, Fiber-reinforced composites, Musculoskeletal mineralized tissues, Effective coefficients

[1] Dipartimento di Scienze Matematiche "G. L. Lagrange", Politecnico di Torino, 10129. Torino, Italia
[2] School of Mathematics and Statistics, Mathematics and Statistics Building, University of Glasgow, University Place, Glasgow G128QQ, UK
[3] Departamento de Matemáticas, Facultad de Matemática y Computación, Universidad de La Habana, CP 10400, La Habana, Cuba

**Corresponding author:**
Ariel Ramírez-Torres, Dipartimento di Scienze Matematiche "G. L. Lagrange", Politecnico di Torino, 10129. Torino, Italia.
Email: ariel.ramirez@polito.it

## Introduction

Hierarchical solids are multiscale materials made of different phases which themselves exhibit a finer scale structure. Several examples of the existence of hierarchical composite structures can be found in nature such as musculoskeletal mineralized tissues (MMTs), lotus leaves, among many others. Nowadays, the study of the physical properties of multiscale composite materials is of great interest due to its utility, for instance, in the modeling and design of bioinspired and biomimetic hierarchical materials[1–3]. In particular, MMTs constitute a widely studied class of hierarchical composite materials. For instance, we refer to the compilation of articles edited by Cowin[4] on structural and mechanical properties of bone.

The different homogenization techniques used in the modeling of multiscale composites have the important advantage of decoupling the structural characteristic lengths. In the case of linear elastic composite materials, the scientific literature develops in two main approaches, the asymptotic homogenization and the average field theory (see, e.g., the review paper[5] and references therein). On one hand, average field techniques[6,7] aim to find the effective elastic properties which relate the fine scale strain and stress averages over a representative volume, characterizing, in an ideal form, the material heterogeneity. On the other hand, the asymptotic homogenization technique[8–12] exploits the scales separation among the characteristic lengths of the local structures and the one of the whole material by employing multiple scale expansions of the fields.

Multiscale asymptotic homogenization techniques take advantage of the information available at the smaller scales to obtain an effective description of the medium or phenomenon at its larger scales. In the scientific literature, there exist several works focusing on modeling and simulation of the macroscopic properties of hierarchical composite materials using average field techniques[13–16], reiterated asymptotic homogenization[9,17–25] and hybrid models[26]. For instance, starting from the basic equations of the phases of a composite featuring a heterogeneous structure over several separated scales,[17] achieved to deduce the phenomenological equations of a porous medium and, in the process, the authors also obtained the governing equations for the intermediate scales of the mixture. Afterwards, a rigorous foundation of the technique was given in[18] focused on the heat equation for composites and in[27], a further generalization of reiterated homogenization was introduced via a three-scale convergence approach providing a groundwork where the asymptotic parameters independently approach zero. Moreover, in[22], the authors adopted an asymptotic homogenization technique to obtain a homogenized model for a fluid saturated porous medium containing double porous substructures by considering a hierarchical porous arrangement. In[23], recurrent sequences of local and averaged elasticity problems for a fiber reinforced composite were written through the introduction of a power series expansion for each level. Furthermore, in[24], the authors considered a hierarchical laminated composite with the particularity that the microstructure presented a combination of linear and non-linear generalized periodicity. Therein, the solution of the problem was sought via a multi-step homogenization approach. In addition, a step-by-step approach to study the properties of bone using models of micromechanics and composite laminate theory was followed in[15] and[16]. Finally, the approach in[26] presents a combination of Eshelby based techniques with the asymptotic homogenization to analyze in a bottom-up process the stiffening of old bone tissues. From a computational point of view, the work by[28] proposes a methodology for the development of adaptive methods for hierarchical modeling of elastic heterogeneous bodies.

In this work, we exploit the three-scale asymptotic homogenization approach developed in[29,30] to investigate the effective properties of linear elastic, hierarchical, fiber-reinforced composites. The three-scale homogenization approach permits to individualize each hierarchical level and to investigate how the properties at the lower scales influence the effective ones in a single scheme. In a previous work[29], the three-scale asymptotic technique has been applied to compute the effective shear modulus for hierarchical fiber-reinforced composites. Here, we go further and propose a procedure to compute the effective in-plane elastic coefficients, which involve the solution of coupled elastic problems. Furthermore, we show the potential of the multiscale asymptotic homogenization process by applying it to a biological scenario of interest. Specifically, we are interested in modeling the effective properties of MMTs by performing a parametric analysis of the mineral crystals' volume fraction. Since the goal is to offer a modeling tool for studying hierarchical composites, we conviniently adopt the modeling assumptions made in[31,26]. In[31], the authors studied the elastic stiffness tensor of a mineralized turkey leg tendon tissue using a multiscale model based on average fields Eshelby techniques, such as the Mori-Tanaka and the self-consistent schemes. In[26], the approach in[31] was extended to the asymptotic homogenization technique by means of a hybrid hierarchical modeling framework applicable to MMTs, and capable to account for fused mineral structures in the composite tissue. The results of the present framework are consistent with the experimental and theoretical data reported in[26,31].

The manuscript is organized as follows. First, the physical and mathematical framework of the problem is introduced. Next, we present the principal results of the three-scale asymptotic homogenization technique and we address the general local problems associated with each hierarchical level. The in-plane and out-of-plane local problems for uniaxially fiber-reinforced hierarchical composites with isotropic constituents are also specified. In addition, the form of the effective coefficients is provided. Furthermore, we compute the effective properties of MMTs and compare the results with experimental and numerical data provided in the scientific literature. Finally, we discuss the current approach and give directions for future developments of the study.

## Formulation of the problem

### *Geometrical description*

Let us denote by $\Omega \subset \mathbb{R}^3$ a multiscale composite characterized by three well-separated characteristics lengths (see Fig. 1), namely $\ell_1$, $\ell_2$ and $L$, and introduce the scaling parameters $\varepsilon_1$ and $\varepsilon_2$ as follows,

$$\varepsilon_1 = \frac{\ell_1}{L} \ll 1 \quad \text{and} \quad \varepsilon_2 = \frac{\ell_2}{L} \ll \varepsilon_1. \tag{1}$$

We note that in (1), we have amended a typo on the definition of $\varepsilon_2$ in previous works[29,30]. From relation (1), two formally independent variables are introduced, i.e.

$$\eta = \frac{x}{\varepsilon_1} \quad \text{and} \quad \varsigma = \frac{x}{\varepsilon_2}. \tag{2}$$

In what follows, we consider each field and material property $\Phi^\varepsilon$ to be $\eta$- and $\varsigma$- periodic and we introduce the notation $\Phi^\varepsilon(x) = \Phi(x, \eta, \varsigma)$.

At the first hierarchical level, the composite $\Omega$ comprises two solid constituents and is partitioned into two sub-domains $\Omega_{\mathrm{m}}^{\varepsilon_1}$ and $\Omega_{\mathrm{f}}^{\varepsilon_1}$. The former denotes the host phase (or matrix) and the latter represents a finite collection of disjoints subphases (e.g. inclusions or fibers). Specifically, $\overline{\Omega} = \overline{\Omega}_{\mathrm{m}}^{\varepsilon_1} \cup \overline{\Omega}_{\mathrm{f}}^{\varepsilon_1}$ with $\overline{\Omega}_{\mathrm{m}}^{\varepsilon_1} \cap \Omega_{\mathrm{f}}^{\varepsilon_1} = \Omega_{\mathrm{m}}^{\varepsilon_1} \cap \overline{\Omega}_{\mathrm{f}}^{\varepsilon_1} = \emptyset$ and we denote with $\Gamma^{\varepsilon_1}$ the interface between both constituents $\Omega_{\mathrm{m}}^{\varepsilon_1}$ and $\Omega_{\mathrm{f}}^{\varepsilon_1}$. Furthermore, we denote by $\mathcal{Y}$ the unitary periodic cell containing a portion of the host phase $\mathcal{Y}_{\mathrm{m}}$ and one subphase (or a finite collection of subphases) $\mathcal{Y}_{\rm f}$. We enforce that the constituents of each periodic cell satisfy that $\overline{\mathcal{Y}} = \overline{\mathcal{Y}}_{\rm m} \cup \overline{\mathcal{Y}}_{\rm f}$ with $\overline{\mathcal{Y}}_{\rm m} \cap \mathcal{Y}_{\rm f} = \mathcal{Y}_{\rm m} \cap \overline{\mathcal{Y}}_{\rm f} = \emptyset$, and we indicate with $\Gamma_{\mathcal{Y}}$ the interface between $\mathcal{Y}_{\rm m}$ and $\mathcal{Y}_{\rm f}$.

At the second hierarchical level, we consider that each subphase ${}_i\Omega_{\rm f}^{\varepsilon_1}$ $(i = 1, ..., N)$ is also a composite material with periodic microstructure. We suppose that each subphase ${}_i\Omega_{\rm f}^{\varepsilon_1}$ is composed of a host phase $\Omega_{\rm m}^{\varepsilon_2}$ with a finite number of subphases denoted by $\Omega_{\rm f}^{\varepsilon_2}$. In particular, we assume that for each $i$, ${}_i\overline{\Omega}_{\rm f}^{\varepsilon_1} = \overline{\Omega}_{\rm m}^{\varepsilon_2} \cup \overline{\Omega}_{\rm f}^{\varepsilon_2}$ with $\overline{\Omega}_{\rm m}^{\varepsilon_2} \cap \Omega_{\rm f}^{\varepsilon_2} = \Omega_{\rm m}^{\varepsilon_2} \cap \overline{\Omega}_{\rm f}^{\varepsilon_2} = \emptyset$ and the interface between $\Omega_{\rm m}^{\varepsilon_2}$ and $\Omega_{\rm f}^{\varepsilon_2}$ is denoted with $\Gamma^{\varepsilon_2}$. At this hierarchical level, $\mathcal{Z}$ stands for the unitary periodic cell containing a portion of the host phase indicated with $\mathcal{Z}_{\rm m}$ and one subphase (or a finite collection of subphases) $\mathcal{Z}_{\rm f}$. Analogously to the upper hierarchical level, we set $\overline{\mathcal{Z}} = \overline{\mathcal{Z}}_{\rm m} \cup \overline{\mathcal{Z}}_{\rm f}$, with $\overline{\mathcal{Z}}_{\rm m} \cap \mathcal{Z}_{\rm f} = \mathcal{Z}_{\rm m} \cap \overline{\mathcal{Z}}_{\rm f} = \emptyset$ and we indicate with $\Gamma_{\mathcal{Z}}$ the interface between $\mathcal{Z}_{\rm m}$ and $\mathcal{Z}_{\rm f}$.

In Table 1, we resume the symbols introduced above.

**Table 1.** Symbols and their description.

| Symbol | Description |
|---|---|
| $\Omega$ | Multiscale composite body |
| $\Omega_{\rm m}^{\varepsilon_1}$ $(\Omega_{\rm m}^{\varepsilon_2})$ | Host (or matrix) phase at the $\varepsilon_1$ $(\varepsilon_2)$-hierarchical level |
| $\Omega_{\rm f}^{\varepsilon_1}$ $(\Omega_{\rm f}^{\varepsilon_2})$ | Finite collection of disjoints subphases at the $\varepsilon_1$ $(\varepsilon_2)$-hierarchical level |
| $\Gamma^{\varepsilon_1}$ $(\Gamma^{\varepsilon_2})$ | Interface between constituents $\Omega_{\rm m}^{\varepsilon_1}$ and $\Omega_{\rm f}^{\varepsilon_1}$ $(\Omega_{\rm m}^{\varepsilon_2}$ and $\Omega_{\rm f}^{\varepsilon_2})$ |
| $\mathcal{Y}$ $(\mathcal{Z})$ | Unitary periodic cell at the $\varepsilon_1$ $(\varepsilon_2)$-hierarchical |
| $\mathcal{Y}_{\rm m}$ $(\mathcal{Z}_{\rm m})$ | level portion of $\Omega_{\rm m}^{\varepsilon_1}$ $(\Omega_{\rm m}^{\varepsilon_2})$ contained in the unitary cell $\mathcal{Y}$ $(\mathcal{Z})$ |
| $\mathcal{Y}_{\rm f}$ $(\mathcal{Z}_{\rm f})$ | Finite collection of subphases $\Omega_{\rm f}^{\varepsilon_1}$ $(\Omega_{\rm f}^{\varepsilon_2})$ contained in the unitary cell $\mathcal{Y}$ $(\mathcal{Z})$ |
| $\Gamma_{\mathcal{Y}}$ $(\Gamma_{\mathcal{Z}})$ | Interface between $\mathcal{Y}_{\rm m}$ and $\mathcal{Y}_{\rm f}$ $(\mathcal{Z}_{\rm m}$ and $\mathcal{Z}_{\rm f})$ |

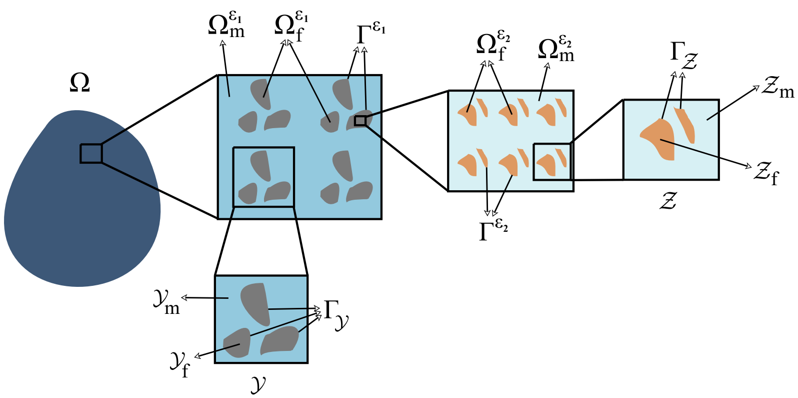


**Figure 1.** Schematic of the cross-section of a hierarchical periodic composite with three structural levels.

## *Formulation of the problem*

We consider that the constitutive response of all the constituents of the hierarchical composite body $\Omega$ is linear elastic. This assumption implies that the constituents' constitutive relationships are all given by the formula,

$$\boldsymbol{\sigma}^{\varepsilon} = \mathscr{C}^{\varepsilon} : \boldsymbol{E}(\boldsymbol{u}^{\varepsilon}), \tag{3}$$

where $\boldsymbol{E}(\boldsymbol{u}^{\varepsilon}) := \mathrm{Sym}\,(\mathrm{Grad}\boldsymbol{u}^{\varepsilon})$ represents the strain tensor under the hypothesis of small displacements $\boldsymbol{u}^{\varepsilon}$, and $\mathscr{C}^{\varepsilon}$ is the fourth-order, positive definite elasticity tensor with both major and minor symmetries, i.e., component-wise, $\mathscr{C}^{\varepsilon}_{ijkl} = \mathscr{C}^{\varepsilon}_{jikl} = \mathscr{C}^{\varepsilon}_{ijlk} = \mathscr{C}^{\varepsilon}_{klij}$ $(i, j, k, l = 1, 2, 3)$, and is supposed to be phase-wise smooth.

Then, ignoring inertia and volume forces, the differential problem arising from the (local) balance of linear momentum when equipped, for example, with Dirichlet-Neumann external boundary conditions reads

$$(\mathscr{P}^{\varepsilon}) \begin{cases} \mathrm{Div}[\mathscr{C}^{\varepsilon} : \boldsymbol{E}(\boldsymbol{u}^{\varepsilon})] = \boldsymbol{0}, & \text{in } \Omega \setminus (\Gamma^{\varepsilon_1} \cup \Gamma^{\varepsilon_2}), \\ \boldsymbol{u}^{\varepsilon} = \boldsymbol{u}^{*}, & \text{on } \partial\Omega_{\mathrm{D}}, \\ [\mathscr{C}^{\varepsilon} : \boldsymbol{E}(\boldsymbol{u}^{\varepsilon})] \cdot \boldsymbol{N} = \boldsymbol{S}^{*}, & \text{on } \partial\Omega_{\mathrm{N}}, \end{cases} \tag{4}$$

where $\boldsymbol{N}$ is the outward unit vector field normal to the boundary $\partial\Omega$ of $\Omega$, $\boldsymbol{u}^{*}$ is the displacement field prescribed on the Dirichlet portion of $\partial\Omega$, i.e., $\partial\Omega_{\mathrm{D}}$, and $\boldsymbol{S}^{*}$ is the field of tractions imposed on the Neumann boundary $\partial\Omega_{\mathrm{N}}$. It holds that $\partial\Omega = \partial\Omega_{\mathrm{D}} \cup \partial\Omega_{\mathrm{N}}$, with $\partial\Omega_{\mathrm{D}} \cap \partial\Omega_{\mathrm{N}} = \emptyset$. Furthermore, continuity conditions for displacements and traction are imposed on both $\Gamma^{\varepsilon_1}$ and $\Gamma^{\varepsilon_2}$, i.e.

$$[\![\boldsymbol{u}^{\varepsilon}]\!] = \boldsymbol{0}, \quad \text{on } \Gamma^{\varepsilon_1} \cup \Gamma^{\varepsilon_2}, \tag{5a}$$

$$[\![(\mathscr{C}^{\varepsilon} : \boldsymbol{E}(\boldsymbol{u}^{\varepsilon})) \cdot \boldsymbol{N}_{\mathcal{Y}}]\!] = \boldsymbol{0}, \quad \text{on } \Gamma^{\varepsilon_1}, \tag{5b}$$

$$[\![(\mathscr{C}^{\varepsilon} : \boldsymbol{E}(\boldsymbol{u}^{\varepsilon})) \cdot \boldsymbol{N}_{\mathcal{Z}}]\!] = \boldsymbol{0}, \quad \text{on } \Gamma^{\varepsilon_2}, \tag{5c}$$

where $\boldsymbol{N}_{\mathcal{Y}}$ and $\boldsymbol{N}_{\mathcal{Z}}$ represent the outward unit vectors normal to the surfaces $\Gamma^{\varepsilon_1}$ and $\Gamma^{\varepsilon_2}$, respectively. The operator $[\![\cdot]\!]$ denotes the jump across the interface between two constituents in the same hierarchical level.

# Three-scale asymptotic homogenization procedure

The property of separation of scales together with definition (2), imply that,

$$\mathrm{Grad}\Phi^{\varepsilon}(x) = \mathrm{Grad}_{x}\Phi(x,\eta,\varsigma) + \varepsilon_1^{-1}\mathrm{Grad}_{\eta}\Phi(x,\eta,\varsigma) + \varepsilon_2^{-1}\mathrm{Grad}_{\varsigma}\Phi(x,\eta,\varsigma), \tag{6}$$

where the chain rule has been used, and the sub-indices of the gradient operators on the right-hand-side indicate that the derivative is performed with respect to $x$, $\eta$, and $\varsigma$. In addition, the following average operators over the periodic cells $\mathcal{Y}$ and $\mathcal{Z}$ are introduced,

$$\langle \Phi^{\varepsilon}(x) \rangle_{\eta} = \frac{1}{|\mathcal{Y}|} \int_{\mathcal{Y}} \Phi(x,\eta,\varsigma)\, d\eta, \tag{7a}$$

$$\langle \Phi^{\varepsilon}(x)\rangle_{\varsigma} = \frac{1}{|\mathcal{Z}|}\int_{\mathcal{Z}} \Phi(x,\eta,\varsigma)\, d\varsigma, \tag{7b}$$

where $|\mathcal{Y}|$ and $|\mathcal{Z}|$ denote the volume fractions of the periodic cells $\mathcal{Y}$ and $\mathcal{Z}$, respectively.

At this stage, we perform a three-scale asymptotic expansion for the displacement $\boldsymbol{u}^{\varepsilon}$ in powers of the scaling parameters $\varepsilon_1$ and $\varepsilon_2$. Specifically, we impose that

$$\boldsymbol{u}^{\varepsilon}(x) = \tilde{\boldsymbol{u}}^{(0)}(x,\eta,\varsigma) + \sum_{i=1}^{+\infty} \tilde{\boldsymbol{u}}^{(i)}(x,\eta,\varsigma)\varepsilon_2^i, \tag{8}$$

where

$$\tilde{\boldsymbol{u}}^{(0)}(x,\eta,\varsigma) = \boldsymbol{u}^{(0)}(x,\eta,\varsigma) + \sum_{j=1}^{+\infty} \boldsymbol{u}^{(j)}(x,\eta,\varsigma)\varepsilon_1^j. \tag{9}$$

Now, we embrace the homogenization process illustrated in[29,30]. That is, we first substitute the expansion (8) into the original problem constituted by equations (4) and (5a)-(5c), and then, we equate the resulting expressions in powers of $\varepsilon_2$, and subsequently, using (9), in powers of $\varepsilon_1$.

Following this procedure, it can be shown that the term $\boldsymbol{u}^{(0)}$ is a function of the "slow" variable only, i.e., $\boldsymbol{u}^{(0)}(x,\eta,\varsigma) \equiv \boldsymbol{u}^{(0)}(x)$, and solution of the *homogenized problem*

$$(\mathscr{P}) \begin{cases} \mathrm{Div}_x[\hat{\mathscr{C}} : \boldsymbol{E}_x(\boldsymbol{u}^{(0)})] = \boldsymbol{0}, & \text{in } \Omega_h, \\ \boldsymbol{u}^{(0)} = \boldsymbol{u}^*, & \text{on } \partial\Omega_{\mathrm{D}}^h, \\ [\hat{\mathscr{C}} : \boldsymbol{E}_x(\boldsymbol{u}^{(0)})]\cdot \boldsymbol{N} = \boldsymbol{S}^*, & \text{on } \partial\Omega_{\mathrm{N}}^h, \end{cases} \tag{10}$$

where $\Omega_h$ represents the homogeneous macro-scale domain in which the homogenized equations are defined. In (10), $\hat{\mathscr{C}}$ represents the *effective fourth-order elasticity tensor* of the hierarchical composite material, which is given by the formula

$$\hat{\mathscr{C}} = \langle \mathscr{C}^{\varepsilon_1} + \mathscr{C}^{\varepsilon_1} : \mathrm{T}\boldsymbol{E}_{\eta}(\boldsymbol{\omega})\rangle_{\eta}, \tag{11}$$

where the fourth-order tensor $\mathscr{C}^{\varepsilon_1}$ is given by

$$\mathscr{C}^{\varepsilon_1}(x) = \begin{cases} \mathscr{C}^{\mathrm{m},\eta}(x,\eta), & \eta \in \Omega_{\mathrm{m}}^{\varepsilon_1}, \\ \mathscr{C}^{\mathrm{f},\eta}(x,\eta), & \eta \in \Omega_{\mathrm{f}}^{\varepsilon_1}. \end{cases} \tag{12}$$

In (12), $\mathscr{C}^{\mathrm{m},\eta}$ and $\mathscr{C}^{\mathrm{f},\eta}$ represent the elasticity tensors corresponding to the constituents $\Omega_{\mathrm{m}}^{\varepsilon_1}$ and $\Omega_{\mathrm{f}}^{\varepsilon_1}$, respectively. Furthermore, $\boldsymbol{\omega}$ is a third-order, $\eta$-periodic tensor field such that

$$\boldsymbol{u}^{(1)}(x,\eta,\varsigma) \equiv \boldsymbol{u}^{(1)}(x,\eta) = \boldsymbol{\omega}(x,\eta) : \boldsymbol{E}_x[\boldsymbol{u}^{(0)}(x)], \tag{13}$$

with $\boldsymbol{E}_x(\boldsymbol{u}^{(0)}(x)) := \mathrm{Sym}[\mathrm{Grad}_x \boldsymbol{u}^{(0)}(x)]$. Moreover, $\mathrm{T}\boldsymbol{E}_{\beta}(\boldsymbol{\omega}) = \frac{1}{2}[\mathrm{TGrad}_{\beta}\boldsymbol{\omega} + {}^{t}(\mathrm{TGrad}_{\beta}\boldsymbol{\omega})]$, with $\beta = x, \eta, \varsigma$ (see[32]). The operation ${}^{t}(\mathscr{A})$ transposes the fourth-order tensor $\mathscr{A}$ by exchanging the order of its first pair of indices only, and $\mathrm{TGrad}_\beta \boldsymbol{\omega}$ is the fourth-order tensor defined as

$$\mathrm{TGrad}_\beta \boldsymbol{\omega} = \frac{\partial \omega_{ikl}}{\partial \beta_j} \boldsymbol{e}_i \otimes \boldsymbol{e}_j \otimes \boldsymbol{e}_k \otimes \boldsymbol{e}_l. \tag{14}$$

Note that we are not using the covariant formalism in this work, otherwise the partial differentiation on the right-hand-side of (14) should be substituted with a covariant derivative.

Particularly, the third-order tensor field $\boldsymbol{\omega}$ is determined by solving the following auxiliary cell problem

$$(\mathscr{P}_{\mathcal{Y}}) \begin{cases} \mathrm{Div}_\eta[\mathscr{C}^{\varepsilon_1} + \mathscr{C}^{\varepsilon_1} : \mathrm{T}\boldsymbol{E}_\eta(\boldsymbol{\omega})] = \boldsymbol{0}, & \text{in } \mathcal{Y} \setminus \Gamma_{\mathcal{Y}}, \\ [\![(\mathscr{C}^{\varepsilon_1} + \mathscr{C}^{\varepsilon_1} : \mathrm{T}\boldsymbol{E}_\eta(\boldsymbol{\omega})) \cdot \boldsymbol{N}_{\mathcal{Y}}]\!] = \boldsymbol{0}, & \text{on } \Gamma_{\mathcal{Y}}, \\ [\![\boldsymbol{\omega}]\!] = \boldsymbol{0}, & \text{on } \Gamma_{\mathcal{Y}}, \end{cases} \tag{15}$$

where the condition $\langle \boldsymbol{\omega} \rangle_\eta = \boldsymbol{0}$ is imposed to guarantee uniqueness in the local problem (15). We remark that the condition of zero average of the third-order tensor $\boldsymbol{\omega}$ is just one particular way, without losing generality, to close the problem (15).

At this point we note that in this formulation (see[29,30] for more details), the homogenization process accomplishes to relate the length scales in a cascade mode from the lower to the higher one, so that, the fourth-order elasticity tensor $\mathscr{C}^{\mathrm{f},\eta}$ in (12), corresponding to the constituent $\Omega_{\mathrm{f}}^{\varepsilon_1}$, is in fact, an effective one, and is given through the formula

$$\mathscr{C}^{\mathrm{f},\eta} \equiv \check{\mathscr{C}} = \langle \mathscr{C}^{\varepsilon_2} + \mathscr{C}^{\varepsilon_2} : \mathrm{T}\boldsymbol{E}_\varsigma(\tilde{\boldsymbol{\omega}}) \rangle_\varsigma. \tag{16}$$

We denote with $\check{\mathscr{C}}$ the *effective fourth-order elasticity tensor at the $\varepsilon_1$-hierarchical level* of the composite material. In particular, for $\eta \in \Omega_{\mathrm{f}}^{\varepsilon_1}$,

$$\mathscr{C}^{\varepsilon_2}(x) = \begin{cases} \mathscr{C}^{\mathrm{m},\varsigma}(x, \eta, \varsigma), & \varsigma \in \Omega_{\mathrm{m}}^{\varepsilon_2}, \\ \mathscr{C}^{\mathrm{f},\varsigma}(x, \eta, \varsigma), & \varsigma \in \Omega_{\mathrm{f}}^{\varepsilon_2}, \end{cases} \tag{17}$$

where $\mathscr{C}^{\mathrm{m},\varsigma}$ and $\mathscr{C}^{\mathrm{f},\varsigma}$ denote the elasticity tensors corresponding to the constituents $\Omega_{\mathrm{m}}^{\varepsilon_2}$ and $\Omega_{\mathrm{f}}^{\varepsilon_2}$, respectively. In (16), $\tilde{\boldsymbol{\omega}}$ is a third-order, $\varsigma-$ and $\eta$-periodic tensor field such that

$$\begin{aligned} \tilde{\boldsymbol{u}}^{(1)}(x, \eta, \varsigma) = \tilde{\boldsymbol{\omega}}(x, \eta, \varsigma) : (\mathscr{I} + \mathrm{T}\boldsymbol{E}_\eta[\boldsymbol{\omega}(x, \eta]) : \boldsymbol{E}_x[\boldsymbol{u}^{(0)}(x)] \\ + \tilde{\boldsymbol{\omega}}(x, \eta, \varsigma) : \mathrm{T}\boldsymbol{E}_x[\boldsymbol{\omega}(x, \eta)] : \boldsymbol{E}_x[\boldsymbol{u}^{(0)}(x)]\varepsilon_1, \end{aligned} \tag{18}$$

where $\mathscr{I}$ is the fourth-order identity tensor, i.e., for every symmetric tensor $\boldsymbol{A}$, it holds that $\mathscr{I} : \boldsymbol{A} = \boldsymbol{A}$. Furthermore, the tensor $\tilde{\boldsymbol{\omega}}$ is solution of the cell problem

$$(\mathscr{P}_{\mathcal{Z}}) \begin{cases} \mathrm{Div}_\varsigma[\mathscr{C}^{\varepsilon_2} + \mathscr{C}^{\varepsilon_2} : \mathrm{T}\boldsymbol{E}_\varsigma(\tilde{\boldsymbol{\omega}})] = \boldsymbol{0}, & \text{in } \mathcal{Z} \setminus \Gamma_{\mathcal{Z}}, \\ [\![(\mathscr{C}^{\varepsilon_2} + \mathscr{C}^{\varepsilon_2} : \mathrm{T}\boldsymbol{E}_\varsigma(\tilde{\boldsymbol{\omega}})) \cdot \boldsymbol{N}_{\mathcal{Z}}]\!] = \boldsymbol{0}, & \text{on } \Gamma_{\mathcal{Z}}, \\ [\![\tilde{\boldsymbol{\omega}}]\!] = \boldsymbol{0}, & \text{on } \Gamma_{\mathcal{Z}}, \end{cases} \tag{19}$$

where the condition $\langle \tilde{\boldsymbol{\omega}} \rangle_\varsigma = \boldsymbol{0}$ is imposed to guarantee uniqueness in the local problem (19).

## Effective properties of hierarchical fiber-reinforced composites

In this section, we particularize the results given in the previous section by focusing on a three-scale composite material with a square-symmetric arrangement of uniaxially aligned cylindrical fibers (see Fig. 2). For this particular case, the three-dimensional cell problems (15) and (19) can be re-formulated as two-dimensional local problems defined over the cells' cross-sections corresponding to a square embedding a single circle.

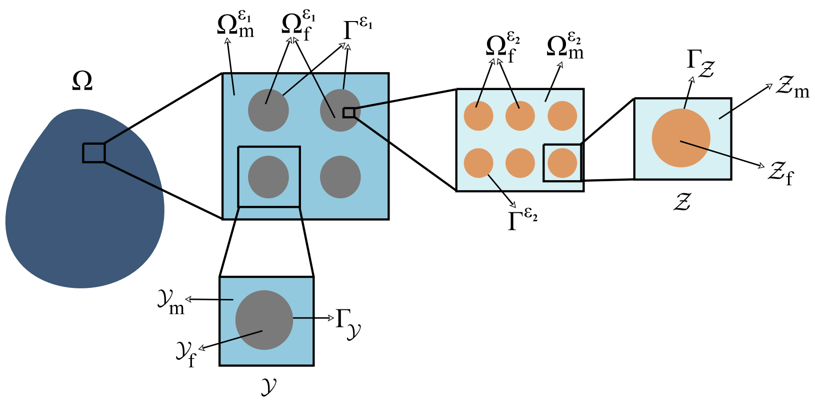


**Figure 2.** Schematic of the cross-section of a hierarchical fiber-reinforced periodic composite with three structural levels.

Specifically, we assume that at the $\varepsilon_2$-hierarchical level, both $\mathscr{C}^{\mathrm{m},\varsigma}$ and $\mathscr{C}^{\mathrm{f},\varsigma}$ are piece-wise constant. This consideration indicates that the dependence of the cell problem $\mathscr{P}_{\mathcal{Z}}$ on $\eta$ and $x$ is lost, and consequently, that the auxiliary third-order tensor $\tilde{\boldsymbol{\omega}}$ depends only on $\varsigma$. Therefore, the effective elasticity tensor at the $\varepsilon_1$-hierarchical level, $\check{\mathscr{C}}$, is likewise piece-wise constant. Additionally, considering that $\mathscr{C}^{\mathrm{m},\eta}$ is piece-wise constant, it can be deduced, in a similar way, that $\boldsymbol{\omega}$ will only depend on $\eta$ and that the effective elasticity tensor, $\hat{\mathscr{C}}$, will be piece-wise constant.

In like manner, we suppose that all the constituents in $\Omega$ are isotropic. This assumption together with the specified geometrical microstructure at the $\varepsilon_2$-hierarchical level implies that $\check{\mathscr{C}}$ is tetragonal symmetric. This means that the effective elasticity tensor $\check{\mathscr{C}}$ has six independent elastic coefficients. Moreover, the assumption of isotropy of the constituent $\Omega_{\mathrm{m}}^{\varepsilon_1}$ induces that the effective coefficient $\hat{\mathscr{C}}$ is at most monoclinic. Therefore, the cell problems $\mathscr{P}_{\mathcal{Z}}$ and $\mathscr{P}_{\mathcal{Y}}$ uncouple in sets of equations for the in-plane and out-of-plane stresses. That is, the local problems (15) and (19) rewrite, each one, as four in-plane problems $\mathscr{P}^{qq}_{\alpha}$ $(q = 1, 2, 3)$ and $\mathscr{P}^{12}_{\alpha}$, with $\alpha = \eta, \varsigma$

$$(\mathscr{P}^{qq}_{\alpha})\begin{cases}\dfrac{\partial\sigma^{qq\gamma,\alpha}_{11}}{\partial\alpha_1}+\dfrac{\partial\sigma^{qq\gamma,\alpha}_{12}}{\partial\alpha_2}=0, & \text{in } \tilde{K}^{\gamma}_{\alpha},\\ \dfrac{\partial\sigma^{qq\gamma,\alpha}_{21}}{\partial\alpha_1}+\dfrac{\partial\sigma^{qq\gamma,\alpha}_{22}}{\partial\alpha_2}=0, & \text{in } \tilde{K}^{\gamma}_{\alpha},\\ [\![\omega^{\alpha}_{1qq}]\!]=0, \quad [\![\omega^{\alpha}_{2qq}]\!]=0, & \text{on } \tilde{\Gamma}_{\alpha},\\ [\![\sigma^{qq,\alpha}_{11}N^{\alpha}_1+\sigma^{qq,\alpha}_{12}N^{\alpha}_2]\!]=-[\![\mathscr{C}^{\alpha}_{11qq}N^{\alpha}_1]\!], & \text{on } \tilde{\Gamma}_{\alpha},\\ [\![\sigma^{qq,\alpha}_{21}N^{\alpha}_1+\sigma^{qq,\alpha}_{22}N^{\alpha}_2]\!]=-[\![\mathscr{C}^{\alpha}_{22qq}N^{\alpha}_2]\!], & \text{on } \tilde{\Gamma}_{\alpha},\end{cases} \tag{20a}$$

$$(\mathscr{P}^{12}_{\alpha})\begin{cases}\dfrac{\partial\sigma^{12\gamma,\alpha}_{11}}{\partial\alpha_1}+\dfrac{\partial\sigma^{12\gamma,\alpha}_{12}}{\partial\alpha_2}=0, & \text{in } \tilde{K}^{\gamma}_{\alpha},\\ \dfrac{\partial\sigma^{12\gamma,\alpha}_{21}}{\partial\alpha_1}+\dfrac{\partial\sigma^{12\gamma,\alpha}_{22}}{\partial\alpha_2}=0, & \text{in } \tilde{K}^{\gamma}_{\alpha},\\ [\![\omega^{\alpha}_{1qq}]\!]=0, \quad [\![\omega^{\alpha}_{2qq}]\!]=0, & \text{on } \tilde{\Gamma}_{\alpha},\\ [\![\sigma^{12\alpha}_{11}N^{\alpha}_1+\sigma^{12\alpha}_{12}N^{\alpha}_2]\!]=-[\![\mathscr{C}^{\alpha}_{1212}N^{\alpha}_2]\!], & \text{on } \tilde{\Gamma}_{\alpha},\\ [\![\sigma^{12\alpha}_{21}N^{\alpha}_1+\sigma^{12\alpha}_{22}N^{\alpha}_2]\!]=-[\![\mathscr{C}^{\alpha}_{1212}N^{\alpha}_1]\!], & \text{on } \tilde{\Gamma}_{\alpha},\end{cases} \tag{20b}$$

and two anti-plane problems $\mathscr{P}^{3q}_{\alpha}$ $(q = 1, 2)$

$$(\mathscr{P}^{3q}_{\alpha})\begin{cases}\dfrac{\partial\sigma^{3q\gamma,\alpha}_{31}}{\partial\alpha_1}+\dfrac{\partial\sigma^{3q\gamma,\alpha}_{32}}{\partial\alpha_2}=0, & \text{in } \tilde{K}^{\gamma}_{\alpha},\\ [\![\omega^{\alpha}_{33q}]\!]=0, & \text{on } \tilde{\Gamma}_{\alpha},\\ [\![\sigma^{3q,\alpha}_{31}N^{\alpha}_1+\sigma^{3q,\alpha}_{32}N^{\alpha}_2]\!]=-[\![\mathscr{C}^{\alpha}_{3131}N^{\alpha}_q]\!], & \text{on } \tilde{\Gamma}_{\alpha},\end{cases} \tag{21}$$

where $\gamma = \mathrm{m}, \mathrm{f}$, and $\tilde{K}^{\gamma}_{\varsigma} := \tilde{\mathcal{Z}}_{\gamma}$ and $\tilde{K}^{\gamma}_{\eta} := \tilde{\mathcal{Y}}_{\gamma}$ denote, respectively, the two-dimensional cross-sections of $\mathcal{Z}_{\gamma}$ and $\mathcal{Y}_{\gamma}$. The interface between the constituents $\tilde{\mathcal{Z}}_{\mathrm{m}}$ and $\tilde{\mathcal{Z}}_{\mathrm{f}}$ ($\tilde{\mathcal{Y}}_{\mathrm{m}}$ and $\tilde{\mathcal{Y}}_{\mathrm{f}}$) is denoted by $\tilde{\Gamma}_{\mathcal{Z}}$ ($\tilde{\Gamma}_{\mathcal{Y}}$).

Additionally, in (20a)–(21)

$$\omega^{\alpha}_{kpq} := \begin{cases}\tilde{\omega}_{kpq}, & \text{for } \alpha = \varsigma,\\ \omega_{kpq}, & \text{for } \alpha = \eta,\end{cases} \tag{22}$$

and

$$\sigma^{pq\gamma,\alpha}_{ij} := \begin{cases}\mathscr{C}^{\gamma,\varsigma}_{ijkl}\dfrac{\partial\tilde{\omega}_{kpq}}{\partial\varsigma_l}, & \text{for } \alpha = \varsigma,\\ \mathscr{C}^{\gamma,\eta}_{ijkl}\dfrac{\partial\omega_{kpq}}{\partial\eta_l}, & \text{for } \alpha = \eta.\end{cases} \tag{23}$$

In (23), $\mathscr{C}^{\gamma,\varsigma}_{ijkl}$ and $\mathscr{C}^{\gamma,\eta}_{ijkl}$ are the components of the elasticity tensor of the constituent $\gamma = \mathrm{m}, \mathrm{f}$ at the $\varepsilon_2$- and $\varepsilon_1$-hierarchical levels, respectively.

Furthermore, component-wise, the fourth-order effective elasticity tensor at the $\varepsilon_1$-hierarchical level $\check{\mathscr{C}}$, and the fourth-order effective elasticity tensor of the hierarchical composite material $\hat{\mathscr{C}}$, are

$$\check{\mathscr{C}}_{ijpq} = \langle \mathscr{C}^{\varepsilon_2}_{ijpq} + \mathscr{C}^{\varepsilon_2}_{ijkl} \frac{\partial \tilde{\omega}_{kpq}}{\partial \varsigma_l} \rangle_\varsigma, \tag{24a}$$

$$\hat{\mathscr{C}}_{ijpq} = \langle \mathscr{C}^{\varepsilon_1}_{ijpq} + \mathscr{C}^{\varepsilon_1}_{ijkl} \frac{\partial \omega_{kpq}}{\partial \eta_l} \rangle_\eta, \tag{24b}$$

respectively.

The theory of analytical functions in[33] applied to the cell problems (20a)-(21) allow us to find the effective coefficients $\check{\mathscr{C}}_{ijpq}$ and $\hat{\mathscr{C}}_{ijpq}$ given in (24a) and (24b), respectively. In the present study we follow the procedure adopted in[34–37] and we adapt it to the obtained scale-coupled cell problems (see Appendix). We note that in the previous work[29] we dealt with the solution of the coupled-anti-plane cell problems, and therefore only the procedure for the coupled-in-plane cell problems is shown. In particular, the choice of the microstructure and material symmetry, and the generality of the analytical approach permit us to focus on the solution of the cell problems in only one hierarchical level. We note that due to the algebraic complexity of the analytical formulae for the effective coefficients given by relations (53a)–(53d) and (55), we use Matlab in order to solve the infinite linear systems (49) and (51), truncated to a fixed order, and, subsequently, to evaluate the results in the corresponding formulae for the effective coefficients.

## Modeling MMTs' effective properties

In the present section we show the potential of the three-scale asymptotic homogenization approach to compute the effective properties of MMTs. Bones and tendons are examples of MMTs, which are hierarchically structured materials, and whose principal constituents, organized spanning several length scales, are mineral crystals, collagen, and water. The principal elements of MMTs are cylindrical mineralized collagen fibrils consisting in self-assembled collagen molecules that are aligned in staggered arrays[31]. The hydroxyapatite crystals are distributed in both the intrafibrillar space, reinforcing the collagen fibrils, and in the extrafibrillar space, which primarily consists of mineral and water (see[31,38] and references therein).

### *Geometrical model for MMTs*

In the present work, we consider an approximated model for MMTs. Specifically, at the $\varepsilon_2$-hierarchical level we suppose that $\mathcal{Z}_\mathrm{m}$ represents the minerals surrounding a single collagen fiber denoted by $\mathcal{Z}_\mathrm{f}$. The collection of all collagen fibers at the $\varepsilon_2$-hierarchical level $\Omega^{\varepsilon_2}_\mathrm{f}$, together with the host phase $\Omega^{\varepsilon_2}_\mathrm{m}$ (representing the minerals) will constitute the mineralized collagen fiber $\mathcal{Y}_\mathrm{f}$ at the $\varepsilon_1$-hierarchical level. The finite collection of mineralized collagen fibers $\Omega^{\varepsilon_1}_\mathrm{f}$ are supposed to be periodically distributed in the extrafibillar space $\Omega^{\varepsilon_1}_\mathrm{m}$. The union of the disjoints sets $\Omega^{\varepsilon_1}_\mathrm{f}$ with $\Omega^{\varepsilon_1}_\mathrm{m}$ will form each one of the mineralized collagen fibril bundles. Finally, the extrafibrillar space is supposed to be a mixture of water and minerals (see Fig. 3). The situation just described, where mineralized collagen fibers are unidirectionally aligned, can be, for example, the case of a mineralized turkey leg tendon, and it can be considered as a simplified model for bones[31].

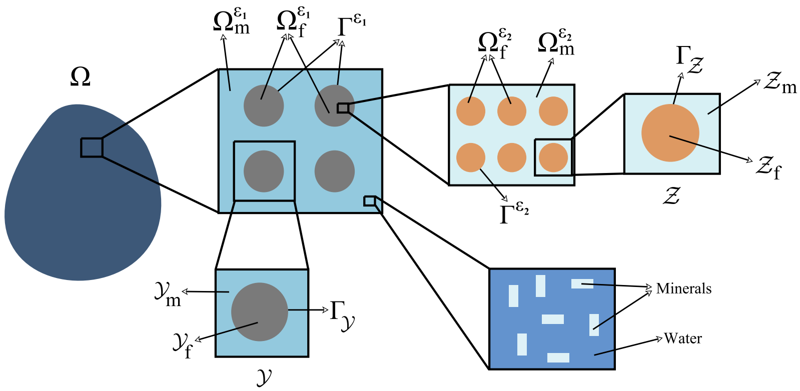


**Figure 3.** Schematic of the cross-section of MMTs.

In order to find the effective properties of the extrafibrillar space we take advantage of Reuss' lower bound formula[39] to compute the effective properties of the mixture $\Omega_{\mathrm{m}}^{\varepsilon_1}$ as follows

$$\mathscr{C}^{\mathrm{m},\eta} = \langle (\mathscr{C}_{\mathrm{ES}})^{-1} \rangle^{-1}, \tag{25}$$

where

$$\mathscr{C}_{\mathrm{ES}}(x) = \begin{cases} \mathscr{C}^{\mathrm{w},\varsigma}(x,\eta,\varsigma), & \text{if } \varsigma \text{ is in the water phase,} \\ \mathscr{C}^{\mathrm{m},\varsigma}(x,\eta,\varsigma), & \text{if } \varsigma \text{ is in the mineral phase.} \end{cases} \tag{26}$$

In (26), $\mathscr{C}^{\mathrm{w},\varsigma}$ and $\mathscr{C}^{\mathrm{m},\varsigma}$ are the elasticity tensors related to the water and mineral phases, respectively. In particular, and following[31], we replace the material properties of water by those of polymethylmethacrylate (PMMA).

We remark that the present three-scale asymptotic approach can be improved to compute the effective properties of the composite extrafibrillar space. However, a realistic geometrical description of the structure of the extrafibrillar space requires numerical simulations in three dimensions for elastic composites (see e.g.[26,40,41]) which are beyond the scope of this work. Here we estimate the effective elastic constants of the extrafibrillar space by means of the Reuss bounds, thus obtaining a fully semi-analytic computational framework at each hierarchical level of organization. Reuss's formula (25) permits to obtain a lower bound for the current model. When we say that we obtain a lower bound for the model, it means that indeed, by considering the asymptotic homogenization approach instead, effective values above those computed using Reuss' scheme are expected[41].

## Effective properties of MMTs

To model the effective properties of MMTs, we conviniently take advantage of some of the modeling assumptions in[31, 26]. Specifically, we consider all constituents of the hierarchical composite material are isotropic and that correspond to those of a bone tissue[31]. That is, Young's modulus ($E$) and Poisson's ratio ($\nu$) of the mineral crystals, collagen fibers and water constituents (individuated by the subscripts $\mathrm{m}$, $\mathrm{c}$ and $\mathrm{p}$, respectively) are given as reported in Table 2.

**Table 2.** Young's modulus and Poisson's ratio of the mineral crystals, collagen fibers and water constituents.

| Parameter | Unit | Value |
|---|---|---|
| $E_{\mathrm{M}}$ | [GPa] | 110 |
| $E_{\mathrm{c}}$ | [GPa] | 5.00 |
| $E_{\mathrm{p}}$ | [GPa] | 4.96 |
| $\nu_{\mathrm{M}}$ | [−] | 0.28 |
| $\nu_{\mathrm{c}}$ | [−] | 0.30 |
| $\nu_{\mathrm{p}}$ | [−] | 0.37 |

Moreover, we perform a parametric analysis of the MMTs' effective properties by increasing the volume fraction of the mineral crystals, denoted by $V$, in the mineralized collagen fibril bundle from $0.2$ to $0.5$ [31]. Following [31], we also take into account the mineral distribution parameter $\phi$, defined as the ratio of the mineral volume in the mineralized collagen fibril to the total mineral volume in the mineralized collagen fibril bundle. In [42], the mineral distribution parameter was estimated to be less than or equal to $0.7$, here we chose $\phi = 0.5$. Specifically, the parameter $\phi$ is related to the phase volume fractions using the following empirical formula [31,43]

$$V^{\mathrm{f},\eta} = \phi V + h(V), \tag{27}$$

where $h(V) := \frac{\varpi}{1+\varpi}(1 - V)$ and $\varpi := 0.36 + 0.084\, e^{6.7V}$. In (27), the symbol $V^{\mathrm{f},\eta}$ represents the volume fraction of the mineralized collagen fibrils in the mineralized collagen fibril bundle. Therefore, the volume fraction of the extrafibrillar space in the mineralized collagen fibril bundle is given by $V^{\mathrm{m},\eta} = 1 - V^{\mathrm{f},\eta}$. Additionally, the volume fractions of the mineral crystals ($V^{\mathrm{m},\zeta}$) and of collagen ($V^{\mathrm{f},\zeta}$) in the mineralized collagen fibril are given by [31]

$$V^{\mathrm{m},\zeta} = \phi \frac{V}{V^{\mathrm{f},\eta}} \quad \text{and} \quad V^{\mathrm{f},\zeta} = 1 - V^{\mathrm{m},\zeta}. \tag{28}$$

Finally, the volume fractions of the mineral crystals and water phases in the extrafibrillar space are

$$V^{\mathrm{f},ES} = (1-\phi)\frac{V}{1 - V^{\mathrm{f},\eta}} \quad \text{and} \quad V^{\mathrm{m},ES} = 1 - V^{\mathrm{f},ES}, \tag{29}$$

respectively.

Figure 4 shows the effective coefficients $[\hat{\mathscr{C}}]_{11}$ (left panel) and $[\hat{\mathscr{C}}]_{33}$ (right panel), obtained by applying the three-scale homogenization approach, plotted with respect to the degree of mineralization of the tissue. In Fig. 4, we also show a comparison with the theoretical results obtained in [31]. Qualitatively, the results are in agreement with the ones obtained by [31], that is, the effective axial and transverse stiffness coefficients increase with respect to the minerals volume fraction. It is known that the results obtained by the asymptotic homogenization method are closer to those obtained by Reuss formula. Therefore, even in this case, we are positive that using an asymptotic approach for the characterization of the composite extrafibrillar space, the effective elastic coefficients will remain close to those in [31].

It is also known that the asymptotic homogenization technique gives effective properties lying between those computed using Reuss and Voigt formulae (see e.g. [41]), which is the case shown in Fig. 4 (right panel), i.e. the results are below those obtained by [31] for $\hat{\mathscr{C}}_{33}$. However, for $\hat{\mathscr{C}}_{11}$, the results lie above

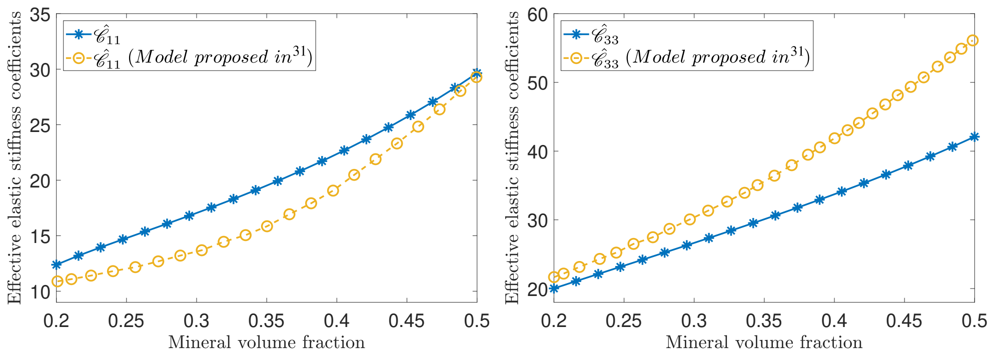


**Figure 4.** Elastic stiffness coefficients $\hat{\mathscr{C}}_{11}$ (left) and $\hat{\mathscr{C}}_{33}$ (right) with respect to the mineral volume fraction $V$. A comparison with the theoretical results in[31] are also shown.

those in[31]. Even though we were not quite expecting this, the curve found with the present approach remains closer to that predicted by[31]. Furthermore, we obtain a satisfactory agreement with experimental data, and actually the obtained bounds are tighter than those in[31], as shown by Fig 5. In Fig. 5, we compare the effective axial and transverse stiffness coefficients with the experimental data showed in[31] corresponding to mineralized turkey leg tendon, human femur and mice bone. As commented before, the results fit very well the experimental data. We note that a Voigt formulation for computing the extrafibrillar space's effective properties is also plausible. Indeed, we also considered Voigt upper bounds to model the properties of the extrafibrillar space. However, we preferred not to show them since the results did not match well the experimental and theoretical data.

The results shown in Fig. 5 could be of special interest for clinical applications including, for instance, tissue reconstruction. Indeed, following the methodology presented in this work, and considering other internal structures and properties, we could assess, in principle, how well fabricated a composite is by matching our analytical/computational results with the real properties of a target tissue (see e.g.[44]). Since the present homogenization approach takes into consideration three spatial scales, with respect to two-scale methods, it provides a better "microscope" to resolve the internal structure of a composite and to capture its material properties.

For completeness in the analysis we show in Fig. 6 the shear effective elastic coefficients $\hat{\mathscr{C}}_{44}$, $\hat{\mathscr{C}}_{55}$ and $\hat{\mathscr{C}}_{66}$ with respect to the mineral volume fraction. As shown in Fig. 6, the shear coefficients $\hat{\mathscr{C}}_{44}$, $\hat{\mathscr{C}}_{55}$ and $\hat{\mathscr{C}}_{66}$ increase with increasing tissue's mineralization. Furthermore, the coefficients $\hat{\mathscr{C}}_{44}$ and $\hat{\mathscr{C}}_{55}$ coincide. We remark that the homogenized elasticity tensor has tetragonal symmetry (6 independent elastic coefficients), i.e. the matrix representation of $\hat{\mathscr{C}}$ (in Voigt notation) is

$$[\hat{\mathscr{C}}] = \begin{pmatrix} \hat{\mathscr{C}}_{11} & \hat{\mathscr{C}}_{12} & \hat{\mathscr{C}}_{13} & 0 & 0 & 0 \\ \hat{\mathscr{C}}_{12} & \hat{\mathscr{C}}_{11} & \hat{\mathscr{C}}_{13} & 0 & 0 & 0 \\ \hat{\mathscr{C}}_{13} & \hat{\mathscr{C}}_{13} & \hat{\mathscr{C}}_{33} & 0 & 0 & 0 \\ 0 & 0 & 0 & \hat{\mathscr{C}}_{44} & 0 & 0 \\ 0 & 0 & 0 & 0 & \hat{\mathscr{C}}_{44} & 0 \\ 0 & 0 & 0 & 0 & 0 & \hat{\mathscr{C}}_{66} \end{pmatrix}. \tag{30}$$

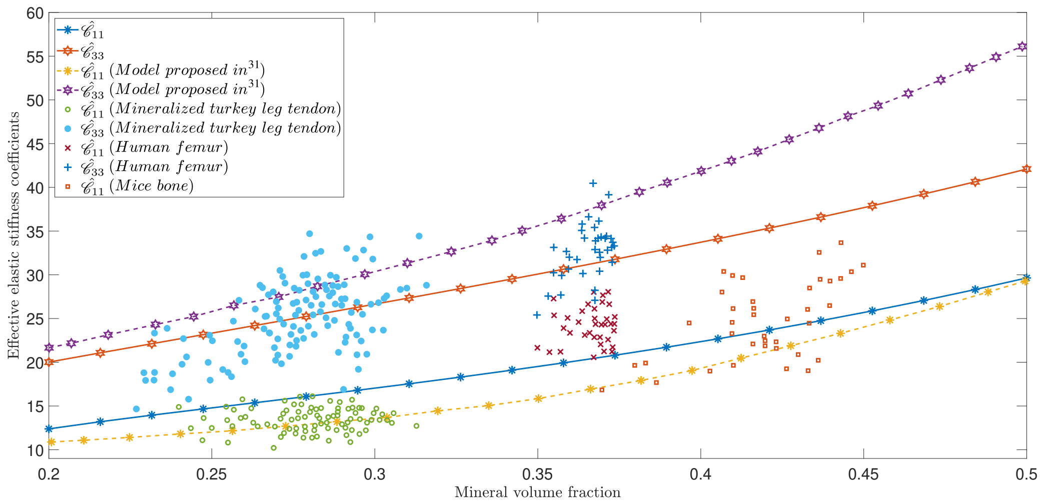


**Figure 5.** Comparison of the predicted and measured elastic stiffness coefficients $\hat{\mathscr{C}}_{11}$ (transverse) and $\hat{\mathscr{C}}_{33}$ (axial) with the experimental and theoretical data reported in[31] (and references therein) corresponding to mineralized turkey tendon leg, human femur and mice bone.

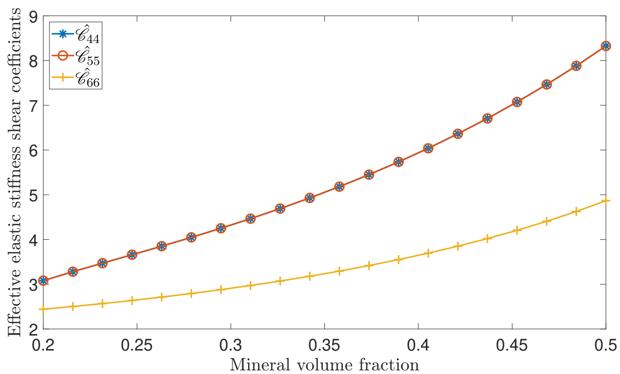


**Figure 6.** Shear effective elastic stiffness coefficients plotted with respect to the mineral volume fraction.

We now turn the attention to the computation of the effective Young's modulus ($\hat{E}$), shear modulus ($\hat{\mu}$) and Poisson's ratio ($\hat{\nu}$) of the hierarchical composite tissue. In particular, the effective shear modulus for hierarchical fiber-reinforced composites has been recently studied in the previous work[29]. Here, we adapt the computational scheme developed therein to the present framework. In the present study, via the homogenization process, the resulting homogenized mineralized tissue shows characteristics of a tetragonal material. Therefore, using Voigt notation, we have that

$$\hat{E}_1 = \frac{\Delta}{(\hat{\mathscr{C}}_{23})^2 - \hat{\mathscr{C}}_{22}\hat{\mathscr{C}}_{33}}, \qquad \hat{\nu}_{12} = \hat{\nu}_{21} = \frac{\hat{\mathscr{C}}_{13}\hat{\mathscr{C}}_{23} - \hat{\mathscr{C}}_{12}\hat{\mathscr{C}}_{33}}{(\hat{\mathscr{C}}_{23})^2 - \hat{\mathscr{C}}_{22}\hat{\mathscr{C}}_{33}}, \tag{31a}$$

$$\hat{E}_2 = \frac{\Delta}{(\hat{\mathscr{C}}_{13})^2 - \hat{\mathscr{C}}_{11}\hat{\mathscr{C}}_{33}}, \qquad \hat{\nu}_{13} = \hat{\nu}_{31} = \frac{\hat{\mathscr{C}}_{12}\hat{\mathscr{C}}_{23} - \hat{\mathscr{C}}_{13}\hat{\mathscr{C}}_{22}}{(\hat{\mathscr{C}}_{23})^2 - \hat{\mathscr{C}}_{22}\hat{\mathscr{C}}_{33}}, \tag{31b}$$

$$\hat{E}_3 = \frac{\Delta}{(\hat{\mathscr{C}}_{12})^2 - \hat{\mathscr{C}}_{11}\hat{\mathscr{C}}_{22}}, \qquad \hat{\nu}_{23} = \hat{\nu}_{32} = \frac{\hat{\mathscr{C}}_{12}\hat{\mathscr{C}}_{13} - \hat{\mathscr{C}}_{11}\hat{\mathscr{C}}_{23}}{(\hat{\mathscr{C}}_{13})^2 - \hat{\mathscr{C}}_{11}\hat{\mathscr{C}}_{33}}, \tag{31c}$$

where

$$\Delta = (\hat{\mathscr{C}}_{13})^2\hat{\mathscr{C}}_{22} - 2\hat{\mathscr{C}}_{12}\hat{\mathscr{C}}_{13}\hat{\mathscr{C}}_{23} + \hat{\mathscr{C}}_{11}(\hat{\mathscr{C}}_{23})^2 + (\hat{\mathscr{C}}_{12})^2\hat{\mathscr{C}}_{33} - \hat{\mathscr{C}}_{11}\hat{\mathscr{C}}_{22}\hat{\mathscr{C}}_{33}. \tag{32}$$

Figure 7 shows the predicted effective Young's moduli (top left), shear moduli (top right) and Poisson's ratio (bottom). We remark that it has been difficult to find experimental data measuring the anisotropic properties of MMTs and validating the computations reported in Fig. 7. Additionally, as details regarding the mineral content in the tissue are often not available in experimental studies, we cannot establish a logical correspondence with the numerical results shown in Fig. 7, as we did previously in Fig. 5. However, in what follows, we make a qualitative comparison with the data available in the scientific literature. In this respect, bone has been an extensively discussed hierarchical tissue, and several experimental techniques, such as micromechanical tests or nanoindentation[45], have been used in the measurement of its mechanical properties. For instance, the experimental studies conducted in[46] for bone tissues show that the magnitude of Young's and shear moduli increase with the degree of mineralization. This trend is captured by our computations as shown in Fig. 7 (top left and top right panels). In addition, Young's moduli and Poisson's ratio of single trabeculae in three orthogonal material directions were measured in[47] using compression tests. Therein, it was reported Young's modulus values in the trabeculae longitudinal direction significantly higher than those on the transverse directions. This experimental findings are in agreement with the predicted results from the present theoretical approach as shown in Fig. 7 (top left panel). Moreover, the data collected in the review paper[45] shows Young's modulus of trabecular bone varying between $0$ Gpa ando $25$ Gpa (see Fig. 5 of[45]), which is in the range of the results obtained for low mineral concentrations. Finally, we observe that $\hat{\nu}_{12}$ decreases, and that $\hat{\nu}_{13} = \hat{\nu}_{23}$ increases, with the augment of tissue's mineralization.

## Conclusions

In the present work we have depicted a three-scale asymptotic homogenization procedure to investigate the effective properties of multiscale, linear elastic composite materials. Using this approach we compute the effective properties of a linear elastic, fiber reinforced hierarchical material using an analytical resolution process, allowing us to reduce the computational cost necessary to calculate the homogenized properties. Furthermore, the three-scale scheme was employed in a biological scenario of interest, that is, the modeling of the macroscopic behavior of MMTs. Specifically, we conducted a parametric study by varying the mineralization of the heterogeneous tissue, and we compared the effective axial and transverse elastic stiffnes constants with theoretical and experimental values. In the study, we take advantage of

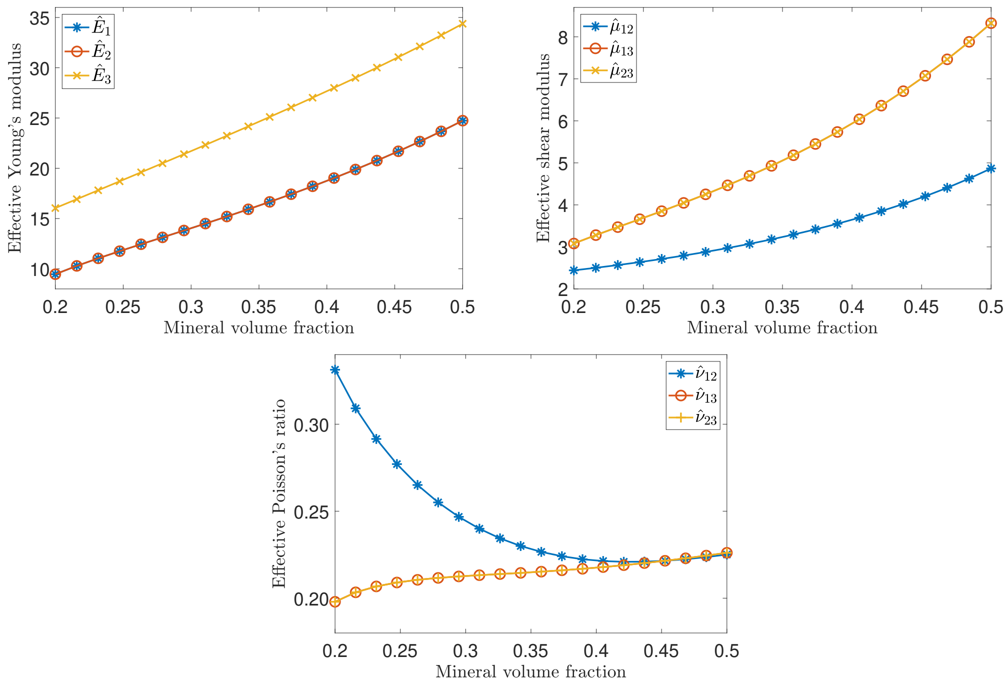


**Figure 7.** Comparison of the predicted effective Young's modulus, shear modulus and Poisson's ratio of the musculoskeletal mineralized tissue with respect to the mineral volume fraction. (Top) $\hat{E}_1$, $\hat{E}_2$ and $\hat{E}_3$, (middle) $\hat{\mu}_{12}$, $\hat{\mu}_{13}$ and $\hat{\mu}_{23}$, (bottom) $\hat{\nu}_{12}$, $\hat{\nu}_{13}$ and $\hat{\nu}_{23}$.

Reuss' lower formula to model the properties of the extrafibrillar space. In this sense, we hypothesize that performing an asymptotic homogenization approach to describe the extrafibrillar space will produce more accurate outcomes for the description of MMTs. Finally, we computed the effective Young's and shear moduli, and Poisson's ratio, and we showed that the predictions are consistent with experimental findings concerning bone tissues.

Minerals content can substantially affect the macroscopic tissue behavior[15,26,48]. Given the complexity that represents to take into account the shape of the mineral crystals embedded in the water solution, one limitation of this work is related to the fact that we model the effective behavior of the extrafibrillar space using Reuss lower formula. In this direction, we aim to account for another scale in the homogenization process, and to solve the related local problem by means of the finite elements method[26]. Further developments of this work include: $(i)$ the generalization to a nonlinear framework (e.g. considering hyperelasticity)[32,49,50] and $(ii)$ the consideration of growth of the tissue and remodelling of its internal structure[32,50–54]. Another issue that could arise in our formulation is that of a non-macroscopically uniform medium. In other words, a medium in which the periodic cells are not independent of the macroscale and thus, the geometry can be varying over the multiple scales, not only the elastic constants. In this particular case, the generalized Reynold's transport theorem (see e.g.[55]) has to be enforced as done, for instance in[56] and in[57] in the context of poro-mechanics. Alternative approaches that are rapidly emerging in the literature also involve a more explicit definition of the normal vector[58], which has been used to investigate the role of porosity gradients to optimize filter efficiency[59]. Also, the macroscopic uniformity assumption may also not be suitable for modelling peculiar situations, such as, for example, localized deformations and damage phenomena that can violate the periodicity constraint. In this context, hierarchical computational schemes have been developed for overcoming this issue[28,60,61]. In an idealized setting, one may think of reinterpreting the small parameter $\varepsilon_2$ as e.g. the damage length-scale and perform an analytical three-scale homogenization approach.

Finally, we remark that the technique has the advantage of reducing the intrinsic geometrical complexities when studying heterogeneous materials, and it ciphers the constituent's properties at the several scales in the effective coefficients,.

## Acknowledgements

ART gratefully acknowledges the research project "Mathematical multi-scale modeling of biological tissues" (N. 64) financed by the Politecnico di Torino (Scientific Advisor: Alfio Grillo). ART and AG acknowledge the Dipartimento di Scienze Matematiche (DISMA) "G.L. Lagrange" of the Politecnico di Torino, "Dipartimento di Eccellenza 2018–2022" ('Department of Excellence 2018–2022'). RRR acknowledges the funding of Proyecto Nacional de Ciencias Básicas 2016–2018 (Project No. 7515) and to Departamento de Matemáticas y Mecánica, IIMAS and PREI-DGAPA at UNAM.

## References

1. Bae WG, Kim HN, Kim D et al. 25th anniversary article: Scalable multiscale patterned structures inspired by nature: the role of hierarchy. *Advanced Materials* 2013; 26(5): 675–700. DOI:10.1002/adma.201303412.
2. Kim CS, Randow C and Sano T (eds.) *Hybrid and Hierarchical Composite Materials*. Springer International Publishing, 2015. DOI:10.1007/978-3-319-12868-9.
3. Yang W, Chen IH, Gludovatz B et al. Natural flexible dermal armor. *Advanced Materials* 2012; 25(1): 31–48. DOI:10.1002/adma.201202713.
4. Cowin SC (ed.) *Bone Mechanics Handbook*. Second edition ed. CRC Press, 2001. ISBN 0-8493-9117-2.
5. Hori M and Nemat-Nasser S. On two micromechanics theories for determining micro–macro relations in heterogeneous solids. *Mechanics of Materials* 1999; 31(10): 667–682. DOI:10.1016/s0167-6636(99)00020-4.
6. Hill R. Elastic properties of reinforced solids: Some theoretical principles. *Journal of the Mechanics and Physics of Solids* 1963; 11(5): 357–372. DOI:10.1016/0022-5096(63)90036-x.
7. Mura T. *Micromechanics of defects in solids*. Springer Netherlands, 1987. DOI:10.1007/978-94-009-3489-4.
8. Bakhvalov N and Panasenko G. *Homogenisation: Averaging Processes in Periodic Media*. Springer Netherlands, 1989. DOI:10.1007/978-94-009-2247-1.
9. Bensoussan A, Lions JL and Papanicolau G. *Asymptotic Analysis for Periodic Structures*. Elsevier Science, 1978.
10. Cioranescu D and Donato P. *An Introduction to Homogenization*. Oxford University Press, 1999. ISBN 0198565542.
11. Sanchez-Palencia E. *Non-Homogeneous Media and Vibration Theory*. Springer Berlin Heidelberg, 1980. DOI: 10.1007/3-540-10000-8.

12. Auriault JL, Boutin C and Geindreau C (eds.) *Homogenization of Coupled Phenomena in Heterogenous Media*. ISTE, 2009. DOI:10.1002/9780470612033.
13. Milton GW. *The Theory of Composites*. Cambridge University Press, 2002. DOI:10.1017/cbo9780511613357.
14. Bader TK, Hofstetter K, Hellmich C et al. The poroelastic role of water in cell walls of the hierarchical composite "softwood". *Acta Mechanica* 2011; 217(1-2): 75–100. DOI:10.1007/s00707-010-0368-8.
15. Nikolov S and Raabe D. Hierarchical modeling of the elastic properties of bone at submicron scales: The role of extrafibrillar mineralization. *Biophysical Journal* 2008; 94(11): 4220–4232. DOI:10.1529/biophysj.107.125567.
16. Hamed E, Lee Y and Jasiuk I. Multiscale modeling of elastic properties of cortical bone. *Acta Mechanica* 2010; 213(1-2): 131–154. DOI:10.1007/s00707-010-0326-5.
17. Mei CC and Auriault JL. Mechanics of heterogeneous porous media with several spatial scales. *Proceedings of the Royal Society A: Mathematical, Physical and Engineering Sciences* 1989; 426(1871): 391–423. DOI: 10.1098/rspa.1989.0132.
18. Allaire G and Briane M. Multiscale convergence and reiterated homogenisation. *Proceedings of the Royal Society of Edinburgh: Section A Mathematics* 1996; 126(02): 297–342. DOI:10.1017/s0308210500022757.
19. Crolet J, Aoubiza B and Meunier A. Compact bone: Numerical simulation of mechanical characteristics. *Journal of Biomechanics* 1993; 26(6): 677–687. DOI:10.1016/0021-9290(93)90031-9.
20. Telega JJ, Galka A and Tokarzewski S. Application of the reiterated homogenization to determination of effective noduli of a compact bone. *Journal of Theoretical and Applied Mechanics* 1999; 37: 687–706.
21. Lukkassen D and Milton GW. On hierarchical structures and reiterated homogenization. In Cwikel M, Englis M, Kufner A et al. (eds.) *Function Spaces, Interpolation Theory and Related Topics*. De Gruyter, pp. 355–368.
22. Rohan E, Naili S, Cimrman R et al. Multiscale modeling of a fluid saturated medium with double porosity: Relevance to the compact bone. *Journal of the Mechanics and Physics of Solids* 2012; 60(5): 857–881. DOI: 10.1016/j.jmps.2012.01.013.
23. Dimitrienko Y, Dimitrienko I and Sborschikov S. Multiscale hierarchical modeling of fiber reinforced composites by asymptotic homogenization method. *Applied Mathematical Sciences* 2015; 9: 7211–7220. DOI: 10.12988/ams.2015.510641.
24. Tsalis D, Charalambakis N, Bonnay K et al. Effective properties of multiphase composites made of elastic materials with hierarchical structure. *Mathematics and Mechanics of Solids* 2015; 22(4): 751–770. DOI: 10.1177/1081286515612142.
25. Nascimento ES, Cruz ME and Bravo-Castillero J. Calculation of the effective thermal conductivity of multiscale ordered arrays based on reiterated homogenization theory and analytical formulae. *International Journal of Engineering Science* 2017; 119: 205–216. DOI:10.1016/j.ijengsci.2017.06.023.
26. Penta R, Raum K, Grimal Q et al. Can a continuous mineral foam explain the stiffening of aged bone tissue? a micromechanical approach to mineral fusion in musculoskeletal tissues. *Bioinspiration & Biomimetics* 2016; 11(3): 035004. DOI:10.1088/1748-3190/11/3/035004.
27. Trucu D, Chaplain M and Marciniak-Czochra A. Three-scale convergence for processes in heterogeneous media. *Applicable Analysis* 2012; 91(7): 1351–1373. DOI:10.1080/00036811.2011.569498.
28. Zohdi TI, Oden J and Rodin GJ. Hierarchical modeling of heterogeneous bodies. *Computer Methods in Applied Mechanics and Engineering* 1996; 138(1-4): 273–298. DOI:10.1016/s0045-7825(96)01106-1.
29. Ramírez-Torres A, Penta R, Rodríguez-Ramos R et al. Homogenized out-of-plane shear response of three-scale fiber-reinforced composites. *Computing and Visualization in Science* 2018; DOI:10.1007/s00791-018-0301-6.
30. Ramírez-Torres A, Penta R, Rodríguez-Ramos R et al. Three scales asymptotic homogenization and its application to layered hierarchical hard tissues. *International Journal of Solids and Structures* 2018; 130-131:

190–198. DOI:10.1016/j.ijsolstr.2017.09.035.

31. Tiburtius S, Schrof S, Molnár F et al. On the elastic properties of mineralized turkey leg tendon tissue: multiscale model and experiment. *Biomechanics and Modeling in Mechanobiology* 2014; 13(5): 1003–1023. DOI:10.1007/s10237-013-0550-8.
32. Ramírez-Torres A, Stefano SD, Grillo A et al. An asymptotic homogenization approach to the microstructural evolution of heterogeneous media. *International Journal of Non-Linear Mechanics* 2018; DOI:10.1016/j.ijnonlinmec.2018.06.012.
33. Muskhelishvili NI. *Some Basic Problems of the Mathematical Theory of Elasticity*. Springer Netherlands, 1977. DOI:10.1007/978-94-017-3034-1.
34. Pobedrya BE. *Mechanics of composite materials*. Moscow State University Press, Moscow, in Russian, 1984.
35. Rodríguez-Ramos R, Sabina FJ, Guinovart-Díaz R et al. Closed-form expressions for the effective coefficients of a fiber-reinforced composite with transversely isotropic constituents – i. elastic and square symmetry. *Mechanics of Materials* 2001; 33(4): 223–235. DOI:10.1016/s0167-6636(00)00059-4.
36. Sabina FJ, Rodríguez-Ramos R, Bravo-Castillero J et al. Closed-form expressions for the effective coefficients of a fibre-reinforced composite with transversely isotropic constituents. II: Piezoelectric and hexagonal symmetry. *Journal of the Mechanics and Physics of Solids* 2001; 49(7): 1463–1479. DOI:10.1016/s0022-5096(01)00006-0.
37. Bravo-Castillero J, Guinovart-Díaz R, Sabina FJ et al. Closed-form expressions for the effective coefficients of a fiber-reinforced composite with transversely isotropic constituents – II. piezoelectric and square symmetry. *Mechanics of Materials* 2001; 33(4): 237–248. DOI:10.1016/s0167-6636(00)00060-0.
38. Weiner S and Wagner HD. THE MATERIAL BONE: Structure-mechanical function relations. *Annual Review of Materials Science* 1998; 28(1): 271–298. DOI:10.1146/annurev.matsci.28.1.271.
39. Reuss A. Berechnung der Fließgrenze von Mischkristallen auf Grund der Plastizittsbedingung für Einkristalle . *ZAMM - Zeitschrift für Angewandte Mathematik und Mechanik* 1929; 9(1): 49–58. DOI:10.1002/zamm.19290090104.
40. Penta R and Gerisch A. Investigation of the potential of asymptotic homogenization for elastic composites via a three-dimensional computational study. *Computing and Visualization in Science* 2015; 17(4): 185–201. DOI:10.1007/s00791-015-0257-8.
41. Penta R and Gerisch A. The asymptotic homogenization elasticity tensor properties for composites with material discontinuities. *Continuum Mechanics and Thermodynamics* 2017; 29(1): 187–206. DOI:10.1007/s00161-016-0526-x.
42. Alexander B, Daulton TL, Genin GM et al. The nanometre-scale physiology of bone: steric modelling and scanning transmission electron microscopy of collagen-mineral structure. *Journal of The Royal Society Interface* 2012; 9(73): 1774–1786. DOI:10.1098/rsif.2011.0880.
43. Raum K, Cleveland RO, Peyrin F et al. Derivation of elastic stiffness from site-matched mineral density and acoustic impedance maps. *Physics in Medicine and Biology* 2006; 51(3): 747–758. DOI:10.1088/0031-9155/51/3/018.
44. Hollister SJ and Lin CY. Computational design of tissue engineering scaffolds. *Computer Methods in Applied Mechanics and Engineering* 2007; 196(31-32): 2991–2998. DOI:10.1016/j.cma.2006.09.023.
45. Wu D, Isaksson P, Ferguson SJ et al. Young's modulus of trabecular bone at the tissue level: A review. *Acta Biomaterialia* 2018; DOI:10.1016/j.actbio.2018.08.001.
46. Mulder L, Koolstra JH, den Toonder JM et al. Relationship between tissue stiffness and degree of mineralization of developing trabecular bone. *Journal of Biomedical Materials Research Part A* 2008; 84A(2): 508–515. DOI:10.1002/jbm.a.31474.

47. Hong J, Cha H, Park Y et al. Elastic moduli and poisson's ratios of microscopic human femoral trabeculae. In Jarm T, Kramar P and A AZ (eds.) *11th Mediterranean Conference on Medical and Biomedical Engineering and Computing 2007*, *IFMBE Proceedings*, volume 16. Springer Berlin Heidelberg, 2007. pp. 274–277. DOI: 10.1007/978-3-540-73044-6_68.
48. García-Rodríguez J and Martínez-Reina J. Elastic properties of woven bone: effect of mineral content and collagen fibrils orientation. *Biomechanics and Modeling in Mechanobiology* 2016; 16(1): 159–172. DOI: 10.1007/s10237-016-0808-z.
49. Pruchnicki E. Hyperelastic homogenized law for reinforced elastomer at finite strain with edge effects. *Acta Mechanica* 1998; 129(3-4): 139–162. DOI:10.1007/bf01176742.
50. Collis J, Brown DL, Hubbard ME et al. Effective equations governing an active poroelastic medium. *Proceedings of the Royal Society A: Mathematical, Physical and Engineering Science* 2017; 473(2198): 20160755. DOI:10.1098/rspa.2016.0755.
51. Sanz-Herrera J, García-Aznar J and Doblaré M. Micro-macro numerical modelling of bone regeneration in tissue engineering. *Computer Methods in Applied Mechanics and Engineering* 2008; 197(33-40): 3092–3107. DOI:10.1016/j.cma.2008.02.010.
52. Peter MA. Coupled reaction–diffusion processes inducing an evolution of the microstructure: Analysis and homogenization. *Nonlinear Analysis: Theory, Methods & Applications* 2009; 70(2): 806–821. DOI: 10.1016/j.na.2008.01.011.
53. O'Dea RD, Nelson MR, Haj AJE et al. A multiscale analysis of nutrient transport and biological tissue growthin vitro. *Mathematical Medicine and Biology* 2014; 32(3): 345–366. DOI:10.1093/imammb/dqu015.
54. Collis J, Hubbard M and O'Dea R. Computational modelling of multiscale, multiphase fluid mixtures with application to tumour growth. *Computer Methods in Applied Mechanics and Engineering* 2016; 309: 554–578. DOI:10.1016/j.cma.2016.06.015.
55. Holmes MH. *Introduction to Perturbation Methods*. Springer New York, 2013. DOI:10.1007/978-1-4614-5477-9.
56. Penta R, Ambrosi D and Shipley RJ. Effective governing equations for poroelastic growing media. *The Quarterly Journal of Mechanics and Applied Mathematics* 2014; 67(1): 69–91. DOI:10.1093/qjmam/hbt024.
57. Penta R, Ambrosi D and Quarteroni A. Multiscale homogenization for fluid and drug transport in vascularized malignant tissues. *Mathematical Models and Methods in Applied Sciences* 2015; 25(01): 79–108. DOI: 10.1142/s0218202515500037.
58. Bruna M and Chapman SJ. Diffusion in spatially varying porous media. *SIAM Journal on Applied Mathematics* 2015; 75(4): 1648–1674.
59. Dalwadi MP, Griffiths IM and Bruna M. Understanding how porosity gradients can make a better filter using homogenization theory. *Proceedings of the Royal Society A: Mathematical, Physical and Engineering Sciences* 2015; 471(2182): 20150464.
60. Fish J. Multiscale analysis of composite materials and structures. *Composites Science and Technology* 2000; 60(12-13): 2547–2556. DOI:10.1016/s0266-3538(00)00048-8.
61. Ghosh S, Lee K and Raghavan P. A multi-level computational model for multi-scale damage analysis in composite and porous materials. *International Journal of Solids and Structures* 2001; 38(14): 2335–2385. DOI:10.1016/s0020-7683(00)00167-0.
62. Grigolyuk EI and Fil'shtinskii LA. Perforated plates and shells. *Nauka, Moscow, in Russian* 1970; .
63. Sokolnikoff IS. *Mathematical theory of elasticity*. McGraw–Hill, New York, 1956.

64. Kantorovich LV and Krylov VI. *Approximate methods of higher analysis*. Interscience Publishers, Inc., The Netherlands, 1964.

## Solution of the cell problems

Following the procedure given in[34–37], we present an analytical approach to find the solution of the cell problems $\mathscr{P}_{\alpha}^{qq}$ $(q = 1, 2, 3)$ and $\mathscr{P}_{\alpha}^{12}$. In particular, the choice of the microstructure and material symmetry allow us to focus on only one hierarchical level.

### *Theoretical background*

In the present section we list some theoretical results that will be useful in the remainder of the text.

**Definition 1.** *Let* $\mathrm{w}_1$ *and* $\mathrm{w}_2$ *two linearly independent complex numbers on* $\mathbb{R}$*. That is, there not exist two real numbers* $a$ *and* $b$*, with* $a, b \neq 0$ *such that* $a\mathrm{w}_1 + b\mathrm{w}_2 = 0$*. We define a* lattice*, the set of all complex numbers of the form*

$$\mathrm{w} = m\mathrm{w}_1 + n\mathrm{w}_2, \quad m, n \in \mathbb{Z}, \tag{33}$$

*which is denoted by* $L = [\mathrm{w}_1, \mathrm{w}_2]$*.*

**Proposition 1.** *The Laurent series expansion of the* $(k-1)$*-th* $(k = 2, 3, \ldots)$ *derivative of the function Z of Weierstrass* $(\zeta)$ *and Natanzon's function* $(Q)$ *in zero are, respectively,*

$$\zeta^{(k-1)} = \frac{(k-1)!}{z^k} - (k-1)! \sum_{l=1}^{\infty\ o} \Lambda_{kl} z^l \quad \textit{and} \quad Q^{(k-1)} = (k-1)! \sum_{l=1}^{\infty\ o} \mathring{\Lambda}_{kl} z^l, \tag{34a}$$

*where*

$$\Lambda_{kl} = -\binom{k+l-1}{l} R^{k+l} S_{k+l} \quad \textit{and} \quad \mathring{\Lambda}_{kl} = k\binom{k+l}{l} R^{k+l} T_{k+l}. \tag{35}$$

*The superscript "o" over the sum operator indicates that the sum is carried out only over odd natural numbers. The reticulate sums (which contains the geometrical information of the problem) are defined by* $S_{k+l} = \sum_{\mathrm{w}\in L*} \frac{1}{\mathrm{w}^{k+l}}$ $(k + l \geq 2)$ *and* $T_{k+l} = \sum_{\mathrm{w}\in L^*} \frac{\overline{\mathrm{w}}}{\mathrm{w}^{k+l+1}}$ $(k + l \geq 3)$*. The series* $S_{k+l}$ *vanishes when* $k + l$ *is not a multiple of* $4$*. Furthermore, the series* $T_{k+l}$ *vanishes when* $k + l$ *is not of the form* $4t - 1$ *for* $t \in \mathbb{N}$[62]*. Moreover,* $L^*$ *represents the lattice excluding the number* $\mathrm{w} = 0$ *and* $\overline{\mathrm{w}}$ *denotes the conjugate of the complex number* $\mathrm{w}$*.*

**Proposition 2.** *The function Z of Weierstrass and Natanzon's function possess the following properties of quasi-periodicity*

$$\zeta(z + \mathrm{w}_p) - \zeta(z) = \delta_p, \qquad \zeta^{(k)}(z + \mathrm{w}_p) - \zeta^{(k)}(z) = 0, \quad \forall k \geq 1 \tag{36a}$$

$$Q(z + \mathrm{w}_p) - Q(z) = \overline{\mathrm{w}}_p P(z) + \xi_p, \qquad Q^{(k)}(z + \mathrm{w}_p) - Q^{(k)}(z) = \bar{\mathrm{w}}_p P^{(k)}(z), \quad \forall k \geq 1, \tag{36b}$$

*where* $P(z) = -\zeta'(z)$, $\delta_p = 2\zeta(\mathrm{w}_p/2)$ *and* $\xi_p = 2Q(\mathrm{w}_p/2) - \overline{\mathrm{w}}_p P(\mathrm{w}_p/2)$. *Moreover, Legendre's relations are fulfilled, i.e.,*

$$\delta_1 \mathrm{w}_2 - \delta_2 \mathrm{w}_1 = 2\pi i, \tag{37a}$$
$$\delta_1 \overline{\mathrm{w}}_2 - \delta_2 \overline{\mathrm{w}}_1 = \xi_2 \mathrm{w}_1 - \xi_1 \mathrm{w}_2. \tag{37b}$$

**Remark 1.** *In the case of a square array of periodic cells, that is, for* $\mathrm{w}_1 = 1$ *and* $\mathrm{w}_2 = i$, *we have that* $\delta_1 = \pi$, $\delta_2 = -i\pi$, $\xi_1 = -\frac{5S_4}{\pi}$ *and* $\xi_2 = i\frac{5S_4}{\pi}$.

## Solution of the in-plane cell problems $\mathscr{P}^{qq}$

The structure of the in-plane cell problems $\mathscr{P}^{qq}$ $(q = 1, 2, 3)$ given in (20a) is of plane-strain and therefore, the theory of harmonic functions and the Kolosov-Muskhelishvili complex potentials[63] are applicable[34–37]. The Kolosov-Muskhelishvili complex potentials are related to $\omega_{1qq}$ and $\omega_{2qq}$, and to the stress components by means of the formulae,

$$2\mathscr{C}^{\gamma}_{1212}(\omega^{\gamma}_{1qq} + i\omega^{\gamma}_{2qq}) = \chi^{\gamma}\varphi^{qq\gamma} - z(\overline{\varphi^{qq\gamma}})' - \overline{\psi^{\gamma}}, \tag{38a}$$
$$\sigma^{qq\gamma}_{11} + \sigma^{q\gamma}_{22} = 2((\varphi^{qq\gamma})' + (\overline{\varphi^{qq\gamma,\alpha}})'), \tag{38b}$$
$$\sigma^{qq\gamma}_{22} - \sigma^{qq\gamma}_{11} = 2(\bar{z}(\varphi^{qq\gamma})'' + (\psi^{qq\gamma})'), \tag{38c}$$

where $\chi^{\gamma} = 3 - 4\nu^{\gamma}$ and $\nu^{\gamma} = \mathscr{C}^{\gamma}_{1122}/(\mathscr{C}^{\gamma}_{1111} + \mathscr{C}^{\gamma}_{1122})$. The notation $\varphi'$ indicates the derivative of $\varphi$ with respect to the complex variable $z$. Following[34–37], the complex potentials $\varphi^{qq\gamma}$ and $\psi^{qq\gamma}$ can be written as

$$\varphi^{qq\mathrm{m}}(z) = \frac{a^{qq}_0}{R} z + \sum_{k=1}^{\infty\, o} a^{qq}_k R^k \frac{\zeta^{(k-1)}(z)}{(k-1)!}, \qquad \varphi^{qq\mathrm{f}}(z) = \sum_{k=1}^{\infty\, o} \frac{z^k}{R^k} c^{qq}_k, \tag{39a}$$
$$\psi^{qq\mathrm{m}}(z) = \frac{b^{qq}_0}{R} z + \sum_{k=1}^{\infty\, o} b^{qq}_k R^k \frac{\zeta^{(k-1)}(z)}{(k-1)!} + \sum_{k=1}^{\infty\, o} a^{qq}_k R^k \frac{Q^{(k-1)}(z)}{(k-1)!}, \qquad \psi^{qq\mathrm{f}}(z) = \sum_{k=1}^{\infty\, o} \frac{z^k}{R^k} d^{qq}_k, \tag{39b}$$

where $a^{qq}_k$, $b^{qq}_k$ $(k = 0, 1, 2, ...)$, and $c^{qq}_k$, $d^{qq}_k$ $(k = 1, 2, ...)$ are complex coefficients to be determined. The radius of the fiber's circular cross section is denoted with $R$.

Using Proposition 1 the complex potentials $\varphi^{qq\mathrm{m}}$ and $\psi^{qq\mathrm{m}}$ can be rewritten as follows

$$\varphi^{qq\mathrm{m}}(z) = \frac{a^{qq}_0}{R} z + \sum_{l=1}^{\infty\, o} \left( a^{qq}_l \frac{R^l}{z^l} + A^{qq}_l \frac{z^l}{R^l} \right), \tag{40a}$$
$$\psi^{qq\mathrm{m}}(z) = \frac{b^{qq}_0}{R} z + \sum_{l=1}^{\infty\, o} \left( b^{qq}_l \frac{R^l}{z^l} + B^{qq}_l \frac{z^l}{R^l} + \mathring{A}^{qq}_l \frac{z^l}{R^l} \right), \tag{40b}$$

where $A^{qq}_l = \sum_{k=1}^{\infty\, o} \Lambda_{kl} a^{qq}_k$, $B^{qq}_l = \sum_{k=1}^{\infty\, o} \Lambda_{kl} b^{qq}_k$ and $\mathring{A}^{qq}_l = \sum_{k=1}^{\infty\, o} \mathring{\Lambda}_{kl} a^{qq}_k$.

Then, find the solution of problem (20a) is equivalent to determine the unknowns $a^{qq}_k$, $b^{qq}_k$, $c^{qq}_k$ and $d^{qq}_k$. In particular, we show that for computing the effective coefficients, it is sufficient to find $a^{qq}_1$. In the following, we outline in three steps, the procedure in[34–37].

*Step 1:* By taking into account the continuity conditions on $\omega_{1qq}$ and $\omega_{2qq}$ and the two expressions in (38a) for $\gamma = \mathrm{m}$ and $\gamma = \mathrm{f}$, we can deduce that

$$\chi^*(\chi^{\mathrm{m}}\varphi^{qq\mathrm{m}} - z\overline{(\varphi^{qq\mathrm{m}})'} - \overline{\psi^{qq\mathrm{m}}}) = \chi^{\mathrm{f}}\varphi^{qq\mathrm{f}} - z\overline{(\varphi^{qq\mathrm{f}})'} - \overline{\psi^{qq\mathrm{f}}}, \tag{41}$$

where $\chi^* = \mathscr{C}^{\mathrm{f}}_{1212}/\mathscr{C}^{\mathrm{m}}_{1212}$. Furthermore, the continuity conditions for traction on the interface $\tilde{\Gamma} = Re^{i\theta}$, $\theta \in [0, 2\pi]$, lead us to the following relation

$$\begin{aligned}(\sigma_{11}^{qq\mathrm{m}} + 2i\sigma_{12}^{qq\mathrm{m}} - \sigma_{11}^{qq\mathrm{m}})e^{i\theta} - (\sigma_{11}^{qq\mathrm{m}} + \sigma_{22}^{qq\mathrm{m}})e^{-i\theta} + 2\beta_1^{qq}e^{i\theta} - 2\beta_2^{qq}e^{-i\theta}\\ = (\sigma_{22}^{qq\mathrm{f}} + 2i\sigma_{12}^{qq\mathrm{f}} - \sigma_{11}^{qq\mathrm{f}})e^{i\theta} - (\sigma_{11}^{qq\mathrm{f}} + \sigma_{22}^{qq\mathrm{f}})e^{-i\theta},\end{aligned} \tag{42}$$

where

$$\beta_j^{qq} = \begin{cases} \dfrac{[\![\mathscr{C}_{1122}]\!] + (-1)^j[\![\mathscr{C}_{1111}]\!]}{2}, & q = 1,\\ (-1)^j\beta_j^{11}, & q = 2,\\ \dfrac{1 + (-1)^j}{2}[\![\mathscr{C}_{1133}]\!], & q = 3,\end{cases} \tag{43}$$

with $j = 1, 2$.

*Step 2:* Subsequently, let us evaluate (38a) (for $\gamma = \mathrm{m}$) in $z$ and $z + \mathrm{w}_p$ and subtract the results of these evaluations. Using the expansions (40a) and (40b), the properties of quasiperiodicity (36a)–(36b), the periodic properties of the functions involved and Legendre's relations, we obtain that

$$a_0^{qq} + \overline{a_0^{qq}} = [(\tau_2 - \chi^{\mathrm{m}}\tau_1)a_1^{qq} + (\overline{\tau_2} - \chi^{\mathrm{m}}\overline{\tau_1})\overline{a_1^{qq}} + (\tau_3 + \overline{\tau_3})b_1^{qq}]\frac{R^2}{\chi^{\mathrm{m}} - 1}, \tag{44a}$$

$$a_0^{qq} - \overline{a_0^{qq}} = [-(\tau_2 + \chi^{\mathrm{m}}\tau_1)a_1^{qq} + (\overline{\tau_2} + \chi^{\mathrm{m}}\overline{\tau_1})\overline{a_1^{qq}} - (\tau_3 - \overline{\tau_3})b_1^{qq}]\frac{R^2}{\chi^{\mathrm{m}} - 1}, \tag{44b}$$

$$\overline{b_0^{qq}} = (\tau_4\chi^{\mathrm{m}}a_1^{qq} + \overline{\tau_5 a_1^{qq}} - \overline{\tau_6 b_1^{qq}})R^2, \tag{44c}$$

where

$$\tau_1 = (\overline{\mathrm{w}_1\delta_2} - \overline{\mathrm{w}_2\delta_1})/W, \qquad \tau_4 = -(\mathrm{w}_1\delta_2 - \mathrm{w}_2\delta_1)/W, \tag{45a}$$

$$\overline{\tau_2} = (\overline{\mathrm{w}_1\xi_2} - \overline{\mathrm{w}_2\xi_1})/W, \qquad \overline{\tau_5} = (\mathrm{w}_1\overline{\xi_2} - \mathrm{w}_2\overline{\xi_1})/W, \tag{45b}$$

$$\overline{\tau_3} = (\overline{\mathrm{w}_1\delta_2} - \overline{\mathrm{w}_2\delta_1})/W, \qquad \overline{\tau_6} = -(\mathrm{w}_1\overline{\delta_2} - \mathrm{w}_2\overline{\delta_1})/W, \tag{45c}$$

where $W = \overline{\mathrm{w}_1}\mathrm{w}_2 - \mathrm{w}_1\overline{\mathrm{w}_2}$. Furthermore, substituting the Kolosov-Muskhelishvili relationships (38b) and (38c) in equation (42), we obtain

$$z\overline{(\varphi^{qq\mathrm{m}})'} + \overline{\psi^{qq\mathrm{m}}} + \varphi^{qq\mathrm{m}} + \overline{z}\beta_1^{qq} + z\beta_2^{qq} = z\overline{(\varphi^{qq\mathrm{f}})'} + \overline{\psi^{qq\mathrm{f}}} + \varphi^{qq\mathrm{f}}. \tag{46}$$

*Step 3:* Now, substituting the Laurent expansions (40a) and (40b) in (41) and in (46), we obtain the following infinite linear system in the unknowns $\tilde{a}_l^{qq} = a_l^{qq}/(R\beta_2^{qq})$ ($q = 1, 2, 3$ and $l = 1, 3, 5, \ldots$)

$$\tilde{a}_l^{qq} + \mathcal{H}_l^1\tilde{a}_1^{qq} + \mathcal{H}_l^2\overline{\tilde{a}_1^{qq}} + \sum_{k=1}^{\infty\, o}\mathcal{W}_{kl}\tilde{a}_k^{qq} + \sum_{k=1}^{\infty\, o}\mathcal{M}_{kl}\overline{\tilde{a}_k^{qq}} = \mathcal{H}_l^{qq}, \tag{47}$$

where

$$
\begin{aligned}
\mathcal{H}_l^1 &= [2\tau_4\chi^{\mathrm{m}}(\chi^{\mathrm{m}}-1)\beta R^2\delta_{1l} + (\overline{\Lambda_{1l}} - \overline{\tau_6}R^2\delta_{1l})(\tau_2 - \chi^{\mathrm{m}}\tau_1)\mu R^2]/[2(\chi^{\mathrm{m}}-1)], && \text{(48a)}\\
\mathcal{H}_l^2 &= [2\overline{\tau_5}(\chi^{\mathrm{m}}-1)\beta R^2\delta_{1l} + (\overline{\Lambda_{1l}} - \overline{\tau_6}R^2\delta_{1l})(\overline{\tau_2} - \chi^{\mathrm{m}}\overline{\tau_1})\mu R^2]/[2(\chi^{\mathrm{m}}-1)], && \text{(48b)}\\
\mathcal{W}_{kl} &= \chi^{\mathrm{mf}*}\mathcal{V}_{kl} + \tau_l\Upsilon\Lambda_{k1}, && \text{(48c)}\\
\mathcal{M}_{kl} &= \chi^{\mathrm{m}*}\mathcal{N}_{kl} + \tau_l\Upsilon\overline{\Lambda_{k1}}, && \text{(48d)}\\
\mathcal{N}_{kl} &= (l+2)\overline{\Lambda_{k(l+2)}} + k\overline{\Lambda_{(k+2)l}} + \overline{\mathring{\Lambda}_{kl}}, && \text{(48e)}\\
\mathcal{V}_{kl} &= \sum_{j=1}^{\infty\, o}\Lambda_{k(j+2)}\overline{\Lambda_{(j+2)l}}, && \text{(48f)}\\
\mathcal{H}_l^{qq} &= (\theta\beta_1^{qq}/\beta_2^{qq} - \overline{\tau_6}R^2\Upsilon^*)\delta_{1l} + \overline{\Lambda_{1l}}\Upsilon^*, && \text{(48g)}\\
\mu &= \beta\alpha_0^{-1}(1+\chi^*\chi^{\mathrm{m}} - \chi^* - \chi^{\mathrm{f}}), && \text{(48h)}\\
\beta &= (1-\chi^*)(\chi^*\chi^{\mathrm{m}}+1)^{-1}, && \text{(48i)}\\
\alpha_0 &= \chi^*[1 - Re(\tau_3)R^2] + (\chi^{\mathrm{f}}-1)\left[\frac{Re(\tau_3)R^2}{\chi^{\mathrm{m}}-1} + \frac{1}{2}\right], && \text{(48j)}\\
\theta &= -(\chi^*\chi^{\mathrm{m}}+1)^{-1}, && \text{(48k)}\\
\chi^{\mathrm{m}*} &= (1-\chi^*)(\chi^*\chi^{\mathrm{m}}+1)^{-1}, && \text{(48l)}\\
\chi^{\mathrm{mf}*} &= (\chi^{\mathrm{m}*}(\chi^*\chi^{\mathrm{m}} - \chi^{\mathrm{f}}))(\chi^* + \chi^{\mathrm{f}})^{-1}, && \text{(48m)}\\
\Upsilon &= (\chi^{\mathrm{m}*}(1+\chi^*\chi^{\mathrm{m}} - \chi^* - \chi^{\mathrm{f}}))\alpha_0^{-1}, && \text{(48n)}\\
\Upsilon^* &= (\chi^{\mathrm{m}*}(\chi^{\mathrm{f}}-1))(2\alpha_0)^{-1}. && \text{(48o)}
\end{aligned}
$$

In particular, the linear system (47) can be equivalently rewritten as

$$
\begin{pmatrix} \tilde{\mathcal{A}}_r^{qq} \\ \tilde{\mathcal{A}}_i^{qq} \end{pmatrix} = \begin{pmatrix} \mathcal{I} + \breve{\mathcal{M}}_r + \breve{\mathcal{W}}_r & \breve{\mathcal{M}}_i - \breve{\mathcal{W}}_i \\ \breve{\mathcal{M}}_i + \breve{\mathcal{W}}_i & \mathcal{I} + \breve{\mathcal{M}}_r - \breve{\mathcal{W}}_r \end{pmatrix}^{-1} \begin{pmatrix} \mathcal{H}_r^{qq} \\ \mathcal{H}_i^{qq} \end{pmatrix}, \tag{49}
$$

where $\tilde{\mathcal{A}}_r^{qq} = (Re(\tilde{a}_1^{qq}), Re(\tilde{a}_3^{qq}), \ldots)^T$, $\tilde{\mathcal{A}}_i^{qq} = (Im(\tilde{a}_1^{qq}), Im(\tilde{a}_3^{qq}), \ldots)^T$, with $\boldsymbol{a}^T$ denoting the operation of transposition of the vector $\boldsymbol{a}$. Moreover, $\mathcal{I}$ is the infinite identity matrix, $\breve{\mathcal{M}}_r = Re(\breve{\mathcal{M}})$, $\breve{\mathcal{W}}_r = Re(\breve{\mathcal{W}})$, $\breve{\mathcal{M}}_i = Im(\breve{\mathcal{M}})$, $\breve{\mathcal{W}}_i = Im(\breve{\mathcal{W}})$, $\mathcal{H}_r^{qq} = Re(\mathcal{H}^{qq})$ and $\mathcal{H}_i^{qq} = Im(\mathcal{H}^{qq})$, where $Re(\Phi)$ and $Im(\Phi)$ denote the operators that extract the real and imaginary parts of $\Phi$, respectively. The matrices $\breve{\mathcal{M}}$ and $\breve{\mathcal{W}}$ are decomposed additively as follows, $\breve{\mathcal{M}} = \mathcal{U} + \mathcal{M}$ and $\breve{\mathcal{W}} = \mathcal{Q} + \mathcal{W}$, where the components of $\mathcal{U}$ and $\mathcal{Q}$, are given by the following expressions,

$$
\mathcal{U}_{kl} = \begin{cases} [2\tau_4\chi^{\mathrm{m}}(\chi^{\mathrm{m}}-1)\chi^{\mathrm{m}*}R^2\delta_{1l} + (\overline{\Lambda_{11}} - \overline{\tau_6}R^2\delta_{1l})(\tau_2 - \chi^{\mathrm{m}}\tau_1)\Upsilon R^2][2(\chi^{\mathrm{m}}-1)]^{-1}, & k = 1, \\ 0, & k > 1, \end{cases} \tag{50a}
$$

$$
\mathcal{Q}_{kl} = \begin{cases} [2\overline{\tau_5}(\chi^{\mathrm{m}}-1)\chi^{\mathrm{m}*}R^2\delta_{1l} + (\overline{\Lambda_{11}} - \overline{\tau_6}R^2\delta_{1l})(\overline{\tau_2} - \chi^{\mathrm{m}}\overline{\tau_1})\Upsilon R^2][2(\chi^{\mathrm{m}}-1)]^{-1}, & k = 1, \\ 0, & k > 1. \end{cases} \tag{50b}
$$

Equation (49) is an infinite linear system with an infinite number of unknowns for which is possible to obtain a solution by truncation through a convergent sequence of solutions[35–37,64].

### *Solution of the problem* $\mathscr{P}^{12}$

The solution of the in-plane problem $\mathscr{P}^{12}$ (20b) can be found following a similar procedure to the one outlined above. In such a case, the following infinite linear system in the unknowns $\tilde{a}_l^{12}$ $(l = 1, 3, 5, \ldots)$ is obtained

$$\begin{pmatrix} \mathcal{A}_r^{12} \\ \\ \mathcal{A}_i^{12} \end{pmatrix} = \begin{pmatrix} \mathcal{I} + \breve{\mathcal{M}}_r + \breve{\mathcal{W}}_r & \breve{\mathcal{M}}_i - \breve{\mathcal{W}}_i \\ \\ \breve{\mathcal{M}}_i + \breve{\mathcal{W}}_i & \mathcal{I} + \breve{\mathcal{M}}_r - \breve{\mathcal{W}}_r \end{pmatrix}^{-1} \begin{pmatrix} \mathcal{H}_r^{12} \\ \\ \mathcal{H}_i^{12} \end{pmatrix}, \tag{51}$$

where $\tilde{\mathcal{A}}_r^{12} = (Re(\tilde{a}_1^{12}), Re(\tilde{a}_3^{12}), \ldots)^T$, $\tilde{\mathcal{A}}_i^{12} = (Im(\tilde{a}_1^{12}), Im(\tilde{a}_3^{12}), \ldots)^T$, $\mathcal{H}_l^{12} = \theta\beta_1^{12} R\delta_{1l}$ and $\beta_1^{12} = -i(\mathscr{C}_{1212}^{\mathrm{m}} - \mathscr{C}_{1212}^{\mathrm{f}})$.

## Effective coefficients

The fact that $\mathscr{C}^{\varepsilon_2}$ is isotropic, together with the assumption that the cell's cross section corresponds to a square embedding a single circle, induce that the tensor $\breve{\mathscr{C}}$ has tetragonal symmetric structure. This result together with the isotropy assumption of the constituent $\Omega_{\mathrm{m}}^{\varepsilon_1}$ imply that the effective tensor $\hat{\mathscr{C}}$ is at most monoclinic. That is, $\hat{\mathscr{C}}$ has at most 13 independent effective elastic coefficients. In the following, we will consider two elasticity tensors $\mathscr{C}^{\mathrm{m}}$ and $\mathscr{C}^{\mathrm{f}}$ having tetragonal symmetric structure. In this way, the results will apply to both hierarchical levels.

### *The in-plane effective coefficients*

Taking into account the major and minor symmetries of the elasticity tensor, the non-zero effective coefficients corresponding to the in-plane problems $\mathscr{P}^{qq}$ are

$$\hat{\mathscr{C}}_{11qq} = \langle \mathscr{C}_{1111}^{\varepsilon} \frac{\partial \omega_{1qq}}{\partial y_1} + \mathscr{C}_{1122}^{\varepsilon} \frac{\partial \omega_{2qq}}{\partial y_2} + \mathscr{C}_{11qq}^{\varepsilon} \rangle, \tag{52a}$$

$$\hat{\mathscr{C}}_{12qq} = \langle \mathscr{C}_{1221}^{\varepsilon} \frac{\partial \omega_{2qq}}{\partial y_1} + \mathscr{C}_{1212}^{\varepsilon} \frac{\partial \omega_{1qq}}{\partial y_2} \rangle, \tag{52b}$$

$$\hat{\mathscr{C}}_{21qq} = \langle \mathscr{C}_{2121}^{\varepsilon} \frac{\partial \omega_{2qq}}{\partial y_1} + \mathscr{C}_{2112}^{\varepsilon} \frac{\partial \omega_{1qq}}{\partial y_2} \rangle, \tag{52c}$$

$$\hat{\mathscr{C}}_{22qq} = \langle \mathscr{C}_{2211}^{\varepsilon} \frac{\partial \omega_{1qq}}{\partial y_1} + \mathscr{C}_{2222}^{\varepsilon} \frac{\partial \omega_{2qq}}{\partial y_2} + \mathscr{C}_{22qq}^{\varepsilon} \rangle, \tag{52d}$$

$$\hat{\mathscr{C}}_{33qq} = \langle \mathscr{C}_{3311}^{\varepsilon} \frac{\partial \omega_{1qq}}{\partial y_1} + \mathscr{C}_{3322}^{\varepsilon} \frac{\partial \omega_{2qq}}{\partial y_2} + \mathscr{C}_{33qq}^{\varepsilon} \rangle. \tag{52e}$$

We observe that the variable $y$ plays the role of $\eta$ and $\varsigma$ since the procedure to obtain the effective coefficients, for this particular case, is the same.

Working with the expressions (52a)–(52e), applying Green's theorem to find the integrals involved, taking into account the periodicity properties of the involved functions, the continuity conditions on the interface $\tilde{\Gamma}$, the Kolosov-Muskhelishvili formula (38a), the Laurent expansions of $\varphi^{qq\mathrm{m}}$ and $\psi^{qqm}$, the orthogonality property of the system of functions $\{e^{in\theta}\}_{n=-\infty}^{+\infty}$ in the interval $[-\pi, \pi]$, we can write

$$\begin{aligned}
\hat{\mathscr{C}}_{11qq} &= \langle \mathscr{C}_{11qq} \rangle - V_{\mathrm{f}} \beta_2^{11} [\beta_2^{11} [2\chi^* \beta(\chi^{\mathrm{f}} + 1)\mathscr{C}_{1212}^{\mathrm{m}}]^{-1} Re(\chi^{\mathrm{f}} \Xi^{qq} - \overline{\Xi^{qq}}) \\
&\quad + Re((\chi^{\mathrm{m}} + 1)\overline{\tilde{a}_1^{qq}} + \beta_1^{qq} (\beta_2^{qq})^{-1})], && (53a)\\
\hat{\mathscr{C}}_{22qq} &= \langle \mathscr{C}_{22qq} \rangle - V_{\mathrm{f}} \beta_2^{11} [\beta_2^{11} [2\chi^* \beta(\chi^{\mathrm{f}} + 1)\mathscr{C}_{1212}^{\mathrm{m}}]^{-1} Re\left(\chi^{\mathrm{f}} \Xi^{qq} - \overline{\Xi^{qq}}\right) \\
&\quad - Re((\chi^{\mathrm{m}} + 1)\overline{\tilde{a}_1^{qq}} + \beta_1^{qq} (\beta_2^{qq})^{-1})], && (53b)\\
\hat{\mathscr{C}}_{33qq} &= \langle \mathscr{C}_{33qq} \rangle - V_{\mathrm{f}} \beta_2^{33} \beta_2^{qq} [2\chi^* \beta(\chi^{\mathrm{f}} + 1)[\mathscr{C}_{1212}^{\mathrm{m}}]^{-1} Re(\chi^{\mathrm{f}} \Xi^{qq} - \overline{\Xi^{qq}}), && (53c)\\
\hat{\mathscr{C}}_{12qq} &= V_{\mathrm{f}} \beta_2^{qq} Im((\chi^{\mathrm{m}} + 1)\overline{\tilde{a}_1^{qq}} + \beta_1^{qq} (\beta_2^{qq})^{-1}), && (53d)
\end{aligned}$$

where $V_{\mathrm{f}} = \pi R^2$ represents the volume fraction of the circular inclusion and

$$\begin{aligned}
\Xi^{qq} &= \{[(\beta\chi_-^{\mathrm{m}} + \mu\beta_0)\tau_2 - (\beta\chi_-^* + \mu\beta_0)\tau_1\chi^{\mathrm{m}}]R^2\}(\chi^{\mathrm{m}} - 1)^{-1}\tilde{a}_1^{qq} + \{[(\beta\chi_-^* + \mu\beta_0)\overline{\tau_2} \\
&\quad - (\beta\chi_-^{\mathrm{m}} + \mu\beta_0)\overline{\tau_1}\chi^{\mathrm{m}}]R^2\}(\chi^{\mathrm{m}} - 1)^{-1}\overline{\tilde{a}_1^{qq}} + (\beta\chi_+ + \mu\beta_0)\tilde{A}_1^{qq} + (\beta\chi_- + \mu\beta_0)\overline{\tilde{A}_1^{qq}} \\
&\quad + \beta(\chi^{\mathrm{f}} + 1) - 2\beta_0\vartheta, && (54a)\\
\beta_0 &= (\chi^{\mathrm{f}} + 1)\left[\frac{Re(\tau_3)R^2}{\chi^{\mathrm{m}} - 1} + \frac{1}{2})\right] - i\chi^* Im(\tau_3)R^2, && (54b)\\
\chi_-^{\mathrm{m}} &= \chi^{\mathrm{f}} + 1 - \chi^*\chi^{\mathrm{m}} + \chi^*, && (54c)\\
\chi_-^* &= \chi^{\mathrm{f}} + 1 + \chi^*\chi^{\mathrm{m}} - \chi^*. && (54d)
\end{aligned}$$

In (54a), we denote by $\tilde{A}_l^{qq} = \sum_{k=1}^{\infty}{}^{o}\, \Lambda_{kl}\tilde{a}_l^{qq}/(R\beta_2^{qq})$.

Resuming, formulae (53a), (53b), (53c) and (53d) give the effective coefficients $\hat{\mathscr{C}}_{11qq}$, $\hat{\mathscr{C}}_{22qq}$, $\hat{\mathscr{C}}_{33qq}$ and $\hat{\mathscr{C}}_{12qq}$, respectively. As anticipated, the effective coefficients depend solely on the unknowns $a_1^{qq}$.

Finally, proceeding in an analogous way, the only one non-zero effective coefficient corresponding to the in-plane problem $\mathscr{P}^{12}$ is

$$\hat{\mathscr{C}}_{1212} = \mathscr{C}_{1212}^{\mathrm{m}} - [\![\mathscr{C}_{1212}]\!] V_{\mathrm{f}} Im((\chi^{\mathrm{m}} + 1)\tilde{a}_1^{12}). \tag{55}$$